NASA CR-177,347
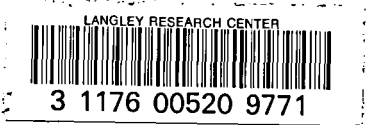
A Reproduced Copy

OF

NASA-CR-177347
19850016901

NASA CR-177,347

Reproduced for NASA

by the

NASA Scientific and Technical Information Facility

FFNo 672 Aug 65

(NASA-CR-177347) ANALYSIS OF SELECTED   N85-25212
PROBLEMS INVOLVING VORTICAL FLOWS (Stanford   THRU
Univ.) 80 p HC A05/MF A01   CSCL 01A   N85-25215
    Unclas
    G3/02   22300

Analysis of Selected Problems Involving Vortical Flows

Leonard Roberts
D. J. Lee
N. Mourtos

NASA

Analysis of Selected Problems Involving Vortical Flows

Leonard Roberts, D. J. Lee and N. Mourtos

Department of Aeronautics and Astronautics
Stanford University, Stanford, California 94305

TABLE OF CONTENTS

I. INTRODUCTION

The importance of vortical flows in a variety of aerodynamic applications is well-known and has been the subject of study for almost a hundred years. Despite numerous theoretical and experimental studies of these flows, however, they are still not fully understood and therefore still continue to gain the attention of the aerodynamicist. In this report three selected problems involving vortical flows are analyzed and discussed, namely

(i) The trailing vortex behind a wing

(ii) Rotor blade-vortex interaction

(iii) The leading edge vortex on a flat plate

On each case a simplified model of the flow is formulated and approximate solutions are found to gain insight into the basic physical phenomena involved.

II. DISCUSSION OF SELECTED PROBLEMS

(i) Trailing Vortex

Vortices appear as a necessary consequence of aerodynamic lift and persist indefinitely, in the absence of laminar or turbulent diffusion, after the passage of an aircraft. In this regard their rate of decay due to diffusion is of practical interest inasmuch as their continued presence behind an aircraft constitutes a potential hazard to following aircraft particularly at low altitude in the terminal area. An analysis of the decay of a vortex pair generated by a wing is given in Appendix A.

The analysis provides approximate closed form solutions for each of two regions (a) a persistence region in which the circumferential flow within the vortex remains unchanged but the axial flow accelerates to the free stream value, and (b) a decay region in which the circumferential flow decays through turbulent diffusion while the axial flow remains at the free stream value.

In particular the analysis provides expressions for the length of persistence of the

vortex before the onset of decay in terms of the aircraft span, wing aspect ratio and lift coefficient. The analysis also gives the vortex radius and velocity profile as a function of distance behind the aircraft.

(ii) Rotor Blade-Vortex Interaction

One of the primary sources of helicopter noise, under certain flight conditions, arises from the interaction of the vortex produced by a blade with the aerodynamics of the following blades. This phenomena, sometimes called blade-slap, is discussed and analyzed in Appendix B. The analysis has three major parts (a) the rotor-tip vortex, (b) the unsteady aerodynamics of the interaction with the following blade, and (c) the acoustic pressure field.

The analysis of the vortex formed by the blade tip includes the effects of turbulence and viscosity at the center of the vortex and therefore does not introduce a singularity as is the case for inviscid vortex models. In the unsteady aerodynamics analysis the disturbance due to the passage of the vortex over the blade is represented as an unsteady gust using a Kutta condition at the trailing edge and the assumption of a flat wake. Acoustic pressures are then determined, using the Hawkings-Ffowcs Williams equation and the results expressed in terms of the vortex characteristics, ie vortex strength, core size and Reynolds number.

A comparison of vortex velocity profiles are found to be in good agreement with experiment. The unsteady lift is found to be dependent on the core size (which in turn varies as the blade radius), on distribution of blade loading and on the Reynolds number based on vortex strength. Extensions of the analysis to determine the effect of spanwise non-compact sources and the effect of variations in blade tip shape on acoustic signature were also undertaken. There appears to be a significant difference between the results of the non-compact source analysis and those for the compact source; even in the far fields there is an appreciable variation in acoustic signature, both in amplitude and shape, depending on observer position. Finally the effect of tip shape on acoustic signature is determined and compared to the effect of tip shape on blade aerodynamics efficiency. Reductions in

acoustic pressure of as much as 6dB may be realized by tip shaping but with an appreciable loss of lifting efficiency (of the order of 20% - 30%).

(iii) Leading Edge Vortex on a Flat Plate

The classical solution for flow over a flat plate in 2-dimensions satisfies a trailing edge Kutta condition but produces a singular behavior at the leading edge. An alternative model has been studied which requires the introduction of a vortex sink placed above the leading edge of the plate. The flow equations are solved and the position and strength of the vortex sink determined in terms of the angle-of-attack of the plate. The solution so found represents the flow near the root of a thin wing where the sink gives rise to a strong spanwise flow contained within the detached vortex, and gives a non-zero drag for the plate.

A comparison is made of this solution with the results of two classical solutions, namely the attached flow with the leading edge singularity and the totally separated flow (Helmholz Solution). The vortex-sink solution is found to exist in the angle of attack range $0 < \alpha < 72°$ with maximum lift occurring at $\alpha = 45°$. This work is given in detail in Appendix C.

III. CONCLUDING REMARKS

The understanding of vortical flows continues to need further improvement in view of the fundamental role they play in a variety of aerodynamic problems and applications. Although much progress has been made in the analysis of inviscid vortical flows there continues to be a lack of complete understanding in areas involving vortical flows interacting with turbulent phenomena. In some cases, as for example in the case of the trailing vortex, such interactions can not be ignored since they determine the rate of vortex decay (and therefore the extent of the hazard to a following aircraft). In other cases, as in the case of the blade vortex interaction, turbulence removes what would otherwise be an inviscid singularity in the pressure at the vortex center, and permits a realistic assessment of the

acoustic signal propagated by the blade. Other problems such as vortex bursting, which lie outside the scope of this report are also of interest in aerodynamic design and deserve increased attention in the future.

N85
25213

UNCLAS

Appendix A

ON THE STRUCTURE OF THE TURBULENT VORTEX

L. Roberts, Stanford University

6

ON THE STRUCTURE OF THE TURBULENT VORTEX

by

Leonard Roberts
Joint Institute for Aeronautics and Acoustic
Durand Bldg · Room 269
Stanford University
Stanford, CA 94305
USA

SUMMARY

This paper provides an analysis that describes the trailing vortex generated by a lifting surface, the structure of its turbulent core and the influence of axial flow within the vortex on its initial persistence and on its subsequent decay. Similarity solutions of the turbulent diffusion equation are given in closed form and results are expressed in sufficiently simple terms that the influence of the lifting surface parameters on the length of persistence and the rate of decay of the vortex can be evaluated readily.

SYMBOLS

A	wing reference area
AR	aspect ratio b^2/A
b	aircraft wing span
b_1	distance between vortices
C_D	induced drag coefficient
C_L	lift coefficient
e	$2\pi r/k^2\Gamma_1$
d	characteristic length of vortex persistence
e	wing lifting efficiency, $C_L^2/\pi AR C_D$
G	$= \frac{\Gamma}{\Gamma_1}$
k	constant, 0.06
l	outer edge of turbulent core
Re	$Ub/\nu AR$
r	distance in radial direction
s	lift distribution parameter, $\int_0^1 \frac{\Gamma}{\Gamma_1} dY$
S	$= \sinh(4s^2/e - 11/12)$
V	velocity function
V^*	maximum value of V
v_θ	circumferential velocity
x	distance in axial direction
$\dot{x}$	x/d
Y	$= y/(b/2)$
y	distance in spanwise direction
z	$= r/r_1(x)$
z^*	$(\xi \log\frac{1}{z})^{\frac{1}{2}}$
Γ	circulation
ϵ	coefficient of eddy viscosity
ν	coefficient of kinetic viscosity
ρ	density

1. INTRODUCTION

The structure of the wake vortex generated by a lifting surface such as an aircraft wing or a rotor blade has been the subject of much previous study, both theoretical and experimental (see for example ref. 1-4). The trailing vortex, after its initial formation is known to comprise two phases, namely (1) a region of persistence for long distances compared to the wing span and (2) a region of decay in which the circumferential velocity is reduced, and the vortex diffuses radially with increasing distance (fig. 1). In this regard it is of particular interest to understand the structure of the vortex in sufficient detail to predict the velocity distribution in the vortex, to explain the initial persistence, and characterize its subsequent rate of decay in terms of the aerodynamic properties of the lifting surface.

2. ANALYSIS

The Potential Flow

The potential flow due to a vortex pair has been analyzed by Spreiter and Sachs (ref 1). In their approach the vortices are considered as a pair of rotating cylinders around which a potential flow exists in the plane normal to the axis of the vortices. The relevant expressions which relate the characteristics of the wing to those of the vortex pair are derived here, for completeness, as follows.

The lift is expressed as

$$L = \frac{1}{2}\rho U^2 C_L A = \rho U b \Gamma_1 \int_0^1 G dY. \tag{1}$$

where Γ_1 is the circulation at the root, $G = \frac{\Gamma}{\Gamma_1}$ is the spanwise distribution of lift, and $Y = \frac{2y}{b}$ is the dimensionless spanwise distance.

The integral in equation (1) is denoted by

$$\int_0^1 G dY = s \tag{2}$$

s is a parameter which characterizes the lift distribution.

The vortex sheet behind the wing rolls into a cylindrical vortex, the inner part of the cylinder containing the vorticity shed from the tip and the outer part containing that shed from the root; thus Γ_1 is the strength of the vortex at its outer edge r_1.

From equation (1), Γ_1 may be written

$$\Gamma_1 = U \frac{b}{2} \frac{C_L}{AR} \cdot \frac{1}{s} \tag{3}$$

where the aspect ratio is $AR = b^2/A$.

Following further the Spreiter-Sachs analysis, the induced drag is related to the rate of formation of rotational kinetic energy in the wake. This relationship is written

$$D = \frac{1}{2}\rho U^2 C_D A = \int \int \frac{1}{2}\rho v_\theta^2 dS' \tag{4}$$

where the integral is performed over the entire plane normal to the direction of flow.

Equations (1) and (4) can be combined to given an expression which relates the energy integral to the wing efficiency

$$\int \int \left(\frac{v_\theta}{\Gamma_1}\right)^2 dS' = \frac{4s^2}{e} \tag{5}$$

where $e = \frac{C_L^2}{\pi AR C_D}$ is the wing efficiency factor.

The integral in equation 5 has contributions from the potential flow outside the vortex pair and from the vortex pair itself; thus

$$\int \int \left(\frac{v_\theta}{\Gamma_1}\right)^2 dS' = \left[\int \int \left(\frac{v_\theta}{\Gamma_1}\right)^2 dS'\right]_{pot} + \frac{1}{\pi}\int_0^{r_1} \left(\frac{\Gamma}{\Gamma_1}\right)^2 \frac{dr}{r} \tag{6}$$

where the substitution $v_\theta = \frac{\Gamma}{2\pi r}$ has been made within the vortex pair.

The contribution from the potential flow is evaluated in closed form and may be written

$$\left[\int \int \left(\frac{v_\theta}{\Gamma_1}\right)^2 dS'\right]_{pot} = \frac{1}{\pi}\sinh^{-1}\frac{b_1}{2r_1} \tag{7}$$

where b_1 is the separation distance between the vortices. The contribution from the vortex pair must be evaluated from the radial distribution of $\frac{\Gamma}{\Gamma_1} = G$ within the vortex. This contribution is found by solving the turbulent flow equations and, as seen later, gives

$$\int_0^r \left(\frac{\Gamma}{\Gamma_1}\right)^2 \frac{dr}{r} = \frac{11}{12} \tag{8}$$

Substitution of (6), (7), and (8) into (5) gives an expression for r_1,

$$r_1 = \frac{b_1}{2} S^{-1} \tag{9}$$

where $S := \sinh(4s^2/e - 11/12)$

The relationship (9) between the vortex radius r_1 and the separation distance b_1 will hold even when r_1 varies with the distance x along the vortex since the flux of rotational energy must be constant and equal to the induced drag at all values of x.

A determination of the separation distance b_1 between the vortices requires that an additional condition be prescribed. It is assumed that the centroid of vorticity is conserved during the roll-up process and thus the initial spanwise separation of the vortex is given by

$$\frac{b_1(0)}{2} = \frac{b}{2}\int_0^1 Y\,dG = \frac{b}{2}s$$

(after integration by parts).

The initial radius of the vortex is

$$r_1(0) = \frac{b}{2}sS^{-1} \tag{10}$$

The initial vortex radius $r_1(0)$ and the circulation Γ_1, given by equation (3) are important parameters in the description of the turbulent core of the vortex as seen in the following analysis.

The Turbulent Vortex Core

For any location x downstream of the lifting surface the characteristics of the vortex will be influenced by turbulence and, to a lesser degree, by kinematic viscosity. There will exist a core within which the circumferential velocity will differ from that given by the potential flow (fig. 2). This vortex core flow can be described by a differential equation expressing the transport of angular momentum as follows:

$$u\frac{\delta G}{\delta x} + v\frac{\delta G}{\delta r} = \frac{r\delta}{\delta r}\left[(\nu + \epsilon)\frac{1}{r}\frac{\delta G}{\delta r}\right] \tag{11}$$

where ν is the kinematic viscosity and ϵ is a turbulent eddy viscosity.

The eddy viscosity for vortex flows has been investigated by Hoffman and Joubert (ref 5) and a model formulated in a way analogous to the traditional mixing length theory of Prandtl. A dimensional analysis suggests that the eddy viscosity is related to the circumferential shear stress through the relationship

$$\epsilon = k\left(\frac{\tau}{\rho}\right)^{\frac{1}{2}} r$$

where

$$\frac{\tau}{\rho} = \epsilon\left(\frac{\delta v_\theta}{\delta r} + \frac{v_\theta}{r}\right)$$

which may be combined to give

$$\epsilon = k^2 r\frac{\delta}{\delta r}(rv_\theta) = \frac{k^2\Gamma_1}{2\pi}r\frac{\delta G}{\delta r} \tag{12}$$

where the constant k must be determined experimentally. The value $k = 0.06$ appears to fit the experimental data.

When equation (12) is substituted into equation (11) the result is written

$$u\frac{\delta G}{\delta x} + v\frac{\delta G}{\delta r} = \frac{k^2\Gamma_1}{2x}r\frac{\delta}{\delta r}\left[\left(c + r\frac{\delta G}{\delta r}\right)\frac{1}{r}\frac{\delta G}{\delta r}\right] \tag{13}$$

where

$$c = \frac{2\pi\nu}{k^2\Gamma_1} = \frac{4\pi}{k^2}\frac{\nu AR}{Ub}\frac{1}{C_L s}$$

(substituting for Γ_1 from equation (3)).

The quantity c is seen to vary inversely with the Reynolds number $\frac{U}{\nu}\frac{b}{AR}$ based on a characteristic chord length, $\frac{b}{AR}$. For a typical aircraft wing c is of the order of 10^{-2} or 10^{-3} and the effects of kinematic viscosity on the overall wake characteristics are negligible. However, in the region close to the center of the vortex (where $r\frac{\delta G}{\delta r} < c$) the effect of viscosity will change the local velocity gradients significantly, creating a "laminar sub-core".

Equation 13 must be solved for the distribution $G(r)$ subject to appropriate boundary conditions, and using suitable approximate expressions for u and v, the convective velocity components. Two cases are considered here corresponding to the region of persistence, where the vortex remains tightly rolled, and the region of decay where the vortex increases its radius and decreases its circumferential velocity with distance along the vortex.

(1) Region of Persistence: Immediately behind the wing it is to be expected that the axial velocity u in the vortex core will be less than the free stream value, U but must accelerate to this value in a distance d say. The velocity components along and normal to the centerline of the vortex may be approximated as

$$\frac{u}{U} = \frac{x}{d}, \quad \frac{v}{U} = -\frac{1}{2}\frac{r}{d} \quad \text{for } x < d$$

satisfying the equation of continuity.

The accelerating flow along the axis (see fig. 3a) causes a radial inflow which in turn convects vorticity inward to balance the outward diffusion by turbulence. This causes the vortex to remain tightly rolled until the axial velocity returns to its free-stream value and the inflow ceases.

(2) Region of Decay: At far distance behind the wing where the axial velocity has recovered to the free stream value

$$\frac{u}{U} = 1, \quad \frac{v}{U} = 0 \quad \text{for } x > d.$$

Here (see fig. 3b) there is no radial inflow but radial diffusion is balanced by axial convection resulting in a spreading of the vortex and as will be seen, a decay in the circumferential velocity, with distance along the vortex.

Approximate Solutions

For both of these regions simple approximate solutions for G can be obtained from equation (11). First it is convenient to define dimensionless variables

$$x = \frac{x}{d}, \quad z = \frac{r}{r_1(x)}, \quad \frac{u}{U} = x^n, \quad \frac{r_1(x)}{r_1(1)} = x^m$$

and seek self similar solutions of the form $G = G(z)$

The resulting ordinary differential equation, derived from equation 13, is written

$$\left[(c + zG')\frac{G'}{z}\right]' + 4\beta^2 G' = 0 \tag{14}$$

where

$$\beta^2 = \frac{1}{4}\left[\frac{\pi U r_1^2(1)}{k^2\Gamma_1 d}\right]\frac{d}{dx}\left[\left(\frac{r_1(x)}{r_1(1)}\right)^2\frac{u(x)}{U}\right] \tag{15}$$

and the prime denotes differentiation with respect to z.

Since β must be independent of x for similarity to hold, the exponents m and n in the expressions for $r_1(x)$ and $u(x)$ respectively must satisfy the relation $2m + n = 1$, thus giving from equation (15).

$$\beta^2 = \frac{1}{4}\pi U r_1^2(1)/k^2\Gamma_1 d \tag{15a}$$

Since $m = \frac{1-n}{2}$, it can be seen that in the region of persistence $(\frac{x}{d} < 1, \frac{h}{U} = \frac{x}{d}, n = 1)$ the corresponding value of m is $m = 0$, so that $r_1(z) = r_1(1) = r_1(0)$. Similarly, in the region of decay $(\frac{x}{d} > 1, \frac{h}{U} = 1, n = 0)$ the value of m is $m = \frac{1}{2}$, so that $r_1(z) = r_1(1)(\frac{x}{d})^{\frac{1}{2}}$.

In order to obtain the solution, $G(z)$, equation (14) must be solved subject to the boundary conditions $G(1) = 1, G'(1) = 0$ (assuming that the core merges with the potential solution ($G \equiv 1$).) and $G(0) = 0$ giving zero circumferential velocity at the center of the vortex.

Equation 14 is nonlinear; however an approximate solution can be found in two steps: since c is a small parameter the solution $\dot{G}$ for $c = 0$ is found valid except for a small region near the center of the vortex where $zG' < c$, and an improved solution, using the approximation $c + zG' = c + z\dot{G}'$, is then found from the resulting linear equation.

Thus, with $c = 0$, equation 14 becomes

$$\left[\dot{G}'\dot{G}'\right]' + 4\beta^2\dot{G}' = 0 \tag{14a}$$

and a solution satisfying the boundary conditions is determined as

$$1 - \dot{G} = (1 - z)^2$$
$$\beta = 1 \tag{10}$$

The term $(c + zG')$ is now approximated as

$$c + zG' \approx c + z\dot{G}' \approx 2(1-z)(z + \frac{c}{2})$$

so that equation 14, with $\beta = 1$, becomes

$$\left[(1-z)(z + \frac{c}{2})\frac{G'}{z}\right]' + 2G' = 0 \tag{14b}$$

Which has the improved solution

$$1 - G = (1 - z)^2\left(1 + \frac{2z}{c}\right)^c \tag{16a}$$
$$\beta = 1$$

Equation 16 closely approximates equation (16a) for small values of c except for $z = 0(c)$, corresponding to a 'laminar subcore' at the center of the vortex.

All of the relevant characteristics of the vortex can now be determined using equation (16a), i.e., the length of persistence, the radius of the turbulent core, the radius of the laminar sub-core, the velocity profiles and the variation of vortex size and velocity with distance x along the axis.

First the integral of equation 8 can now be evaluated using the approximate solution $\dot{G} = 1 - (1 - z)^2$ giving

$$\int_0^{r_1}\left(\frac{\Gamma}{\Gamma_1}\right)^2\frac{dr}{r} = \int_0^1 \dot{G}^2\frac{dz}{z} = \frac{11}{12}$$

thus verifying equation 8.

The characteristic distance of persistence, d is found from 15a, with $\beta = 1$, as

$$d = \frac{\pi}{4}\frac{U}{k^2\Gamma_1}r_1^2(0) \tag{17}$$

The same result, expressed in terms of the aerodynamic parameters of the wing $(b, C_L,$ and $AR)$ is written

$$d = \frac{\pi}{8k^2}\frac{AR}{C_L}s^3S^{-2}b \tag{17a}$$

The radius of the turbulent core r_1 is determined as

$$r_1 = r_1(0) \qquad \text{for } \frac{x}{d} < 1$$
$$\dots (x)^{\frac{1}{2}} \qquad x \tag{18}$$

corresponding to the region of persistence and decay respectively.

Alternatively, in terms of the wing parameters

$$r_1 = sS^{-1}\frac{b}{2} \qquad \text{for } \frac{z}{d} < 1$$

$$= \left(\frac{8k^2}{\pi} \cdot \frac{C_L}{AR}\right)^{\frac{1}{4}} s^{-\frac{1}{4}}\left(\frac{z}{b}\right)^{\frac{1}{4}}\frac{b}{2} \qquad \text{for } \frac{z}{d} > 1 \tag{18a}$$

with d given by equation 17a.

The circumferential velocity v_θ is determined from $v_\theta = \frac{\Gamma}{2\pi r}$ as

$$v_\theta = \frac{\Gamma_1}{2\pi r_1(0)}V(z), \qquad \frac{z}{d} < 1$$

$$= \frac{\Gamma_1}{2\pi r_1(0)}V(z)\left(\frac{z}{d}\right)^{-\frac{1}{4}}, \qquad \frac{z}{d} > 1 \tag{19}$$

where

$$V(z) = \frac{G}{z} = \frac{1 - (1-z)^2\left(1 + \frac{2z}{c}\right)^c}{z}, \qquad z < 1$$

$$V(z) = \frac{1}{z} \qquad z > 1 \tag{20}$$

with $z = \frac{r}{r_1(z)}$ and $r_1(z)$ given by equation (18), d by equation (17).

Alternatively

$$v_\theta = \frac{1}{2\pi}\frac{C_L}{AR}s^{-2}SV(z)U \qquad \text{for } \frac{z}{d} < 1$$

$$= \frac{1}{2}(8\pi k^2)^{-\frac{1}{4}}\left(\frac{C_L}{AR}\right)^{\frac{1}{4}}s^{-\frac{1}{4}}\left(\frac{z}{b}\right)^{-\frac{1}{4}}V(z)U \qquad \text{for } \frac{z}{d} > 1 \tag{19a}$$

with d given by equation (17a). The variation of v_θ with $\frac{z}{d}$ is shown in fig. 4.

The velocity profile $V(z)$ represented by equation 20 has the following characteristics (described in fig. 5):

(a) For $z \ll c, V(z) \approx \frac{2z}{c}$ giving a linear variation with slope $\frac{2}{c}$ near the center of the vortex corresponding to the laminar subcore,

(b) For $c \ll z < 1; V(z) = 2 - z$ corresponding to the turbulent core,

(c) For $z > 1; V(z) = \frac{1}{z}$ corresponding to the potential vortex.

The maximum circumferential velocity is found by differentiation of $V(z)$. For $c \ll 1$ it can be shown that the maximum occurs at $z = z^* = \left(\frac{c}{2}\log\frac{1}{c}\right)^{\frac{1}{2}}$ and has the value

$$V^* = 2 - 2\left(\frac{c}{2}\log\frac{1}{c}\right)^{\frac{1}{2}} \tag{20a}$$

For most purposes, the limiting case $c = 0$ corresponding to infinitely large Reynolds number, can be taken giving

$$V^* = 2 \quad \text{at} \quad z = 0$$

3. RESULTS AND DISCUSSION

The analysis has provided approximate closed-form solutions that describe the structure of the turbulent vortex pair generated by a lifting surface. Two regions of the wake are identified; a region of persistence followed by a region of decay. The initial persistence of the wake is associated with an acceleration of the flow along the axis of the vortex causing a radial inflow which counteracts the outward radial diffusion. When the axial velocity recovers to the free stream value the inflow ceases and the vortex starts to decay.

In the interest of brevity the results discussed here will be primarily for the case of an elliptically loaded wing with brief mention of the influence of inboard and outboard loading which may be determined when the quantities s and $e' = \frac{C_D}{\pi A R C_L^2}$ are known. The general expressions for the quantities of interest are given in equations (17)-(20) which reduce to the simpler forms discussed below with $s = \frac{\pi}{4}$ and $e = 1$ corresponding to elliptic loading.

The length of persistence d for a wing of elliptic loading is given by

$$d = 10.4 \frac{AR}{C_L} b$$

and shows that the length of persistence varies directly as the product of the span and the aspect ratio and inversely as the lift coefficient. For a typical large transport aircraft in a high lift configuration (b=200ft, AR=7 and C_L=1) the length of persistence is approximately 14,000ft (2.65 miles). On the other hand for a typical fighter aircraft (b=50ft, AR=1, C_L=2) the length of persistence is only 250ft.

Considering now a description of the vortex, in the persistence region, the radius of the turbulent core r_1, where the flow departs from the potential vortex is given by

$$r_1 = .175b$$

independent of aspect ratio and lift coefficient. The laminar subcore radius, taken as the location of maximum velocity depends on the Reynolds number and (for elliptical loading) is:

$$r^* = .175 \left(\frac{c}{2} \log \frac{1}{c} \right)^{\frac{1}{4}} b$$

where $c = \frac{4 \times 10^4}{Re}$, $Re = \frac{\Gamma b}{\nu AR}$. For $Re = 10^7$, $c = .004$ the value of r^* is

$$r^* = .018b$$

thus, for a transport aircraft of 200ft span, the maximum velocity occurs near the center of the core at a radius of 3.6ft.

The maximum velocity is given (again for elliptic loading) by

$$v_\theta^* = 1.16 \frac{C_L}{AR} U$$

Thus for the transport aircraft ($AR = 7, C_L = 1$) and U=300ft/sec the maximum velocity near the center of the vortex is 50ft/sec; for a fighter aircraft ($AR = 1, C_L = 2$ and $U = 300$ft/sec) however, the maximum velocity would be 700ft/sec (ignoring compressibility effects).

In the decay region, i.e. for $x > 10.4 \frac{AR}{C_L} b$, the radius of the turbulent core and the subcore grows as $\left(\frac{x}{d} \right)^{\frac{1}{4}}$, i.e.,

$$r_1(x) = .175 \left(\frac{x}{d} \right)^{\frac{1}{4}} b = .054 \left(\frac{C_L}{AR} \right)^{\frac{1}{4}} \left(\frac{x}{b} \right)^{\frac{1}{4}} b$$

and

$$r^*(x) = .054 \left(\frac{C_L}{AR} \right)^{\frac{1}{4}} \left(\frac{c}{2} \log \frac{1}{c} \right)^{\frac{1}{4}} \left(\frac{x}{b} \right)^{\frac{1}{4}} b$$

For the transport aircraft given in the previous example the turbulent core extends to a radius of 70ft at a distance of 10.6 miles behind the aircraft and the radius r^*, at which the maximum velocity occurs, is approximately 7ft. The velocity v_θ at this point is 25ft/sec. For the fighter aircraft the velocity rate of decay with distance is greater (since the velocity reduces by a factor of 2 in a distance $x = 5d$, and d is only 250ft in this case).

From the general equation for d (equation 17a) and v_θ (equation 19a) it can be inferred that configurations which have smaller values of v_θ on the vortex wake (small C_L, large AR, large s)

also have larger distances of persistence, (and those configurations having higher values of v_θ have smaller distance of persistence). Moreover, from 19a it can be seen that in the decay region the only dependence on the span distribution parameter s is $v_\theta \sim s^{-\frac{1}{2}}$, a relatively weak dependence which suggests that the reduction of the high velocities in the far wake through tailoring of the span distribution of lift is not a very promising technique.

Although comparison with experiments is not made in this paper it has been found that the general trends are reasonably well represented by the analysis given here. The dependence of persistence on the axial flow at the center of the vortex probably deserves further analysis, however, including the influence of promoting decay through mass injection thereby permitting the axial flow to recover earlier to free stream conditions.

Finally, application of the solutions given here to rotor wakes also deserves mention. In this regard the effects of Reynolds number on the behavior of the velocity v_θ near the axis of the vortex may be much more important, particularly in a proper description of the interaction of the vortex with a following blade. In this situation the effects of viscosity in the laminar subcore play an essential role in eliminating the singularity in the velocity gradient thereby permitting a realistic calculation of the vortex-blade interaction including the acoustic field so generated.

REFERENCES

1. Spreiter, J. R. and Sachs, A. H.: The rolling up of the trailing vortex sheet and its effect on the downwash behind wings, Journal of the Aeronautical Sciences, vol. 18, no.1, January 1951, pp 21-32.

2. Squire, H. B.: The growth of a vortex in turbulent flow, Aeronautical Quarterly, vol. 16, 1965, pp 3 - 306.

3. Iversen, J. D.: Correlation of turbulent trailing vortex decay data, AIAA Journal of Aircraft, May 1976.

4. Roberts, L.: Persistence and Decay of Wake Vorticity; AGARD Conference on Flight/Ground Testing Facilities Correlation, 1975.

5. Hoffman, E. R. and Joubert, P. N.: Turbulent line vortices, Journal of Fluid Mechanics, vol. 16, 1963, pp. 395-411.

6. Corsiglia, V. R., Schwind, R. G., and Chigier, N. A.: Rapid scanning, three dimensional hot wire anemometer surveys of wing tip vortices, AIAA Journal of Aircraft, vol. 10 no. 12, December 1973, pp 752-757.

7. Donaldson, C. DuP.: Calculation of turbulent shear flow, for atmospheric and vortex motions, AIAA Journal, vol. 10, 1972, pp. 4-12.

8. Tung, C., Pucci, C. S., Caradonna, F. X., and Morse, H. A.: The structure of trailing vortices generated by model rotor modes, NASA TM 81316.
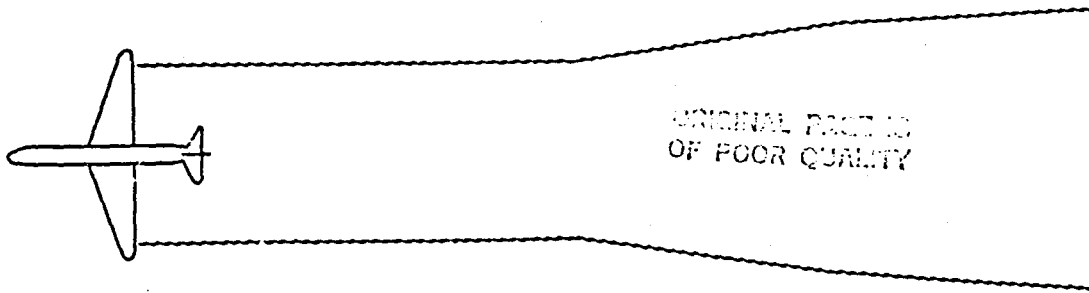
Persistence

Vortex scale and velocity unchanged
with distance behind the aircraft

Decay

Vortex radius increases, and velocity
decreases, with distance behind the
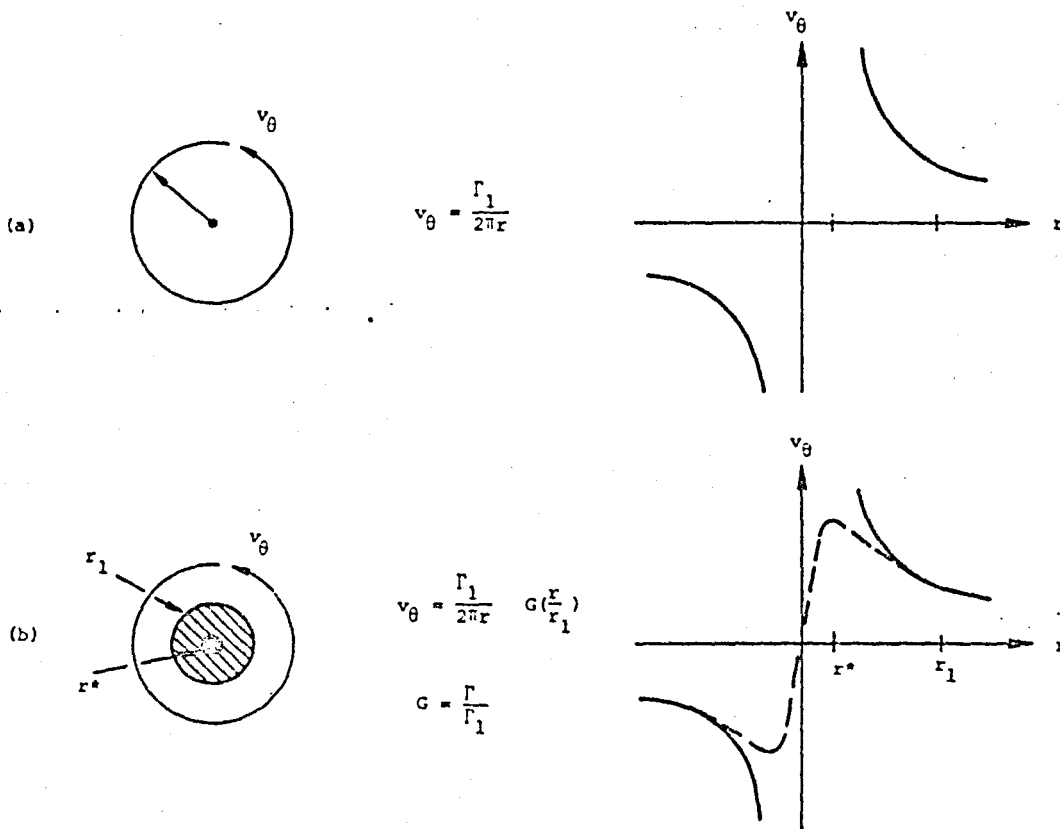aircraft

Fig.1   Trailing vortex flow

(a)

$$v_\theta = \frac{\Gamma_1}{2\pi r}$$

(b)

$$v_\theta = \frac{\Gamma_1}{2\pi r} \quad G\left(\frac{r}{r_1}\right)$$

$$G = \frac{\Gamma}{\Gamma_1}$$

Fig.2   Vortex structure: (a) Potential flow, (b) Turbulent flow,
(r_1 = radius of turbulent core, r^* = radius of laminar subcore)
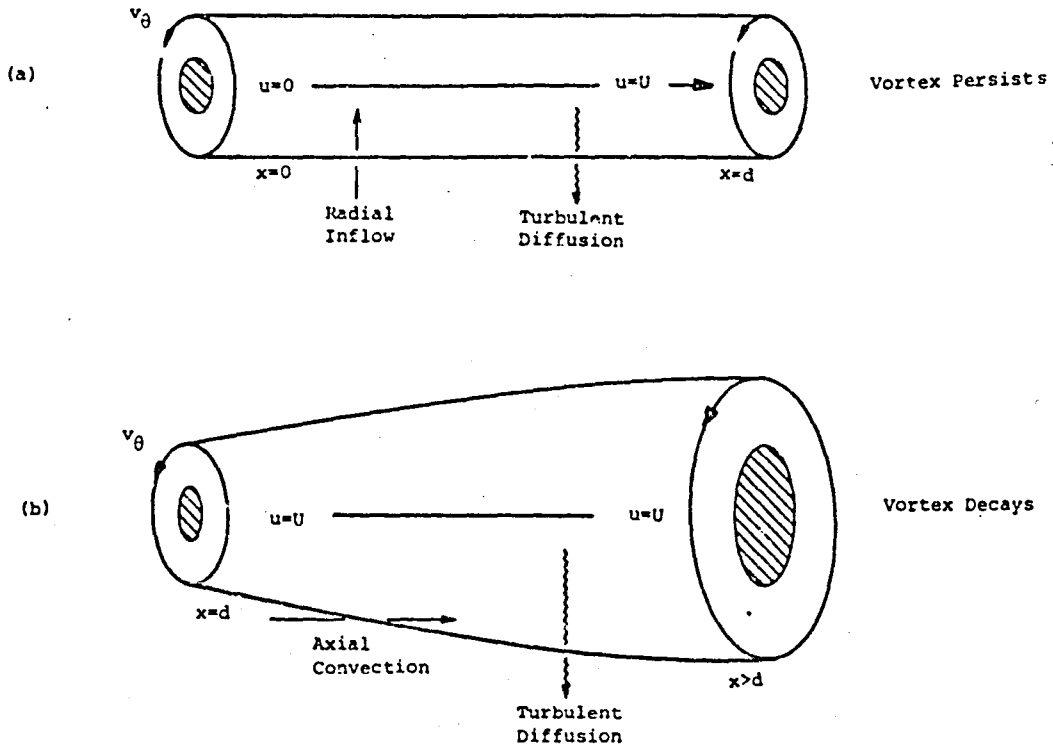
Fig.3 Effect of axial flow on the vortex. (a) Accelerating axial flow, (b) Constant velocity axial flow

$$d = \frac{\pi}{8k^2} \frac{AR}{C_L} s^3 S^{-2} b$$

$$v_\theta^*(0) = \frac{1}{\pi} \frac{C_L}{AR} s^{-2} SU$$
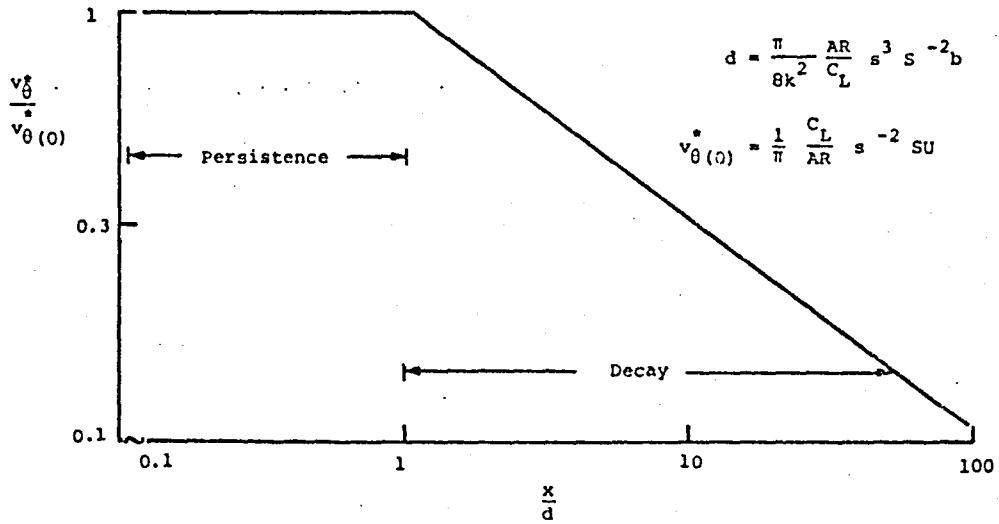
Fig.4 Variation of maximum circumferential velocity with distance behind an aircraft
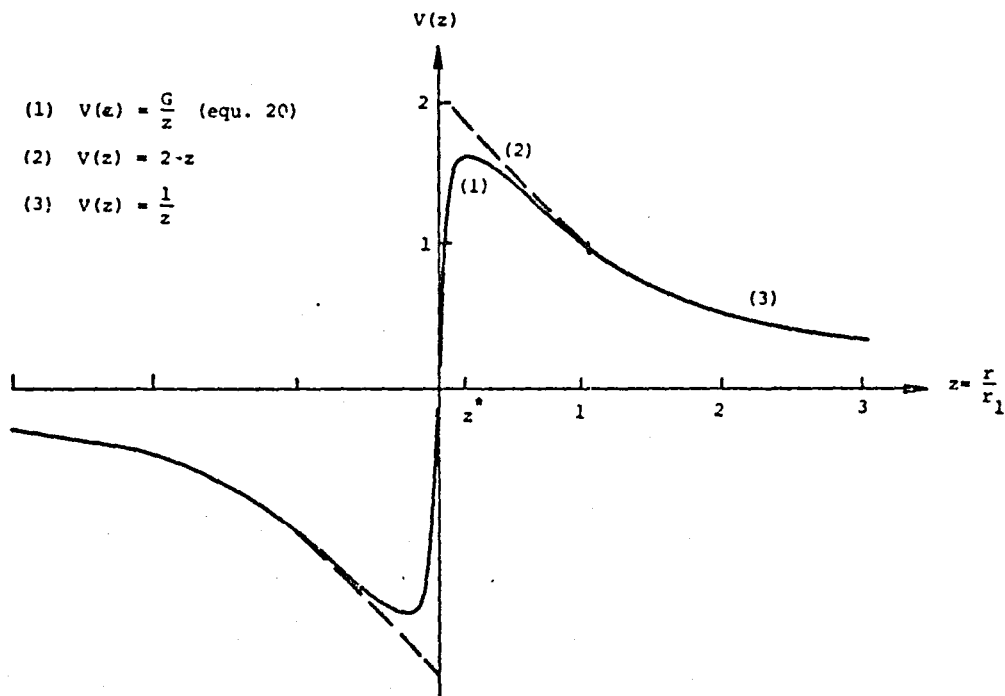
Fig.5   Radial profiles of circumferential velocity

N85
25214

UNCLAS

Appendix B

INTERACTION OF A TURBULENT VORTEX WITH A LIFTING SURFACE

D. J. Lee and L. Roberts, Stanford University., Stanford, CA

INTERACTION OF A TURBULENT VORTEX
WITH A LIFTING SURFACE

D. J. Lee* and L. Roberts+
Joint Institute for Aeronautics and Acoustics
Department of Aeronautics and Astronautics
Stanford University, Stanford, California

ABSTRACT

The impulsive noise due to blade-vortex-interaction is analyzed in the time domain for the extreme case when the blade cuts through the center of the vortex core with the assumptions of no distortion of the vortex path or of the vortex core. An analytical turbulent vortex core model, described in terms of the tip aerodynamic parameters, is used and it's effects on the unsteady loading and maximum acoustic pressure during the interaction are determined.

NOMENCLATURE

a_o	speed of sound in the medium at rest
A_t	equivalent tip area
AR_t	equivalent tip aspect ratio
b	blade semichord
c	nondimensional constant $\frac{?}{2}\frac{\nu}{\Gamma_1}$
$C_{D..}$	induced drag coefficient of the tip
$C_{L.}$	lift coefficient of the tip
$C(k)$	Theodorsen function
d	characteristic length of vortex persistence
d_t	width of the signal in time
ϵ	aerodynamic efficiency $\frac{C_L}{\pi AR C_D}$
j	blade surface function or frequency Hz
G	nondimensional circulation function Γ/Γ_1
J_o, J_1	Bessel function of the first kind of order 0, 1
k	constant 0.06 or reduced frequency $\omega b/U$
l_s	span length of the acoustic source
M	Mach number
n_j	unit vector in j direction
p	acoustic pressure at the position of the observer or pressure on the surface
$p_{.j}$	compressive stress tensor
R	distance between moving source and observer or rotor radius
R_1, R_2, R_3	$\tilde{R}$ component in y_1, y_2, y_3 direction
r, θ, z	cylindrial coordinate
r_t	turbulent vortex core radius
$r_t(0)$	initial r_t
r^*	laminar sub core radius
r_d	half the distance between the equivalent vortex pair
Re	Reynolds number Γ_1/ν
R_m	rotor radius at maximum circulation
R_o	initial distance from the observer and source in y_1 direction
s	nondimensional time $U\tau/b$
s_t	tip loading parameter $s_t = \int_o^1 G dy/(R - R_m)$
S	blade surface
t	reception time (or observed time)
T_o	period of the acoustic signal
U	convecting blade speed
v, v_θ, u	vortex velocity in r, θ, z directions
$V(z)$	vortex velocity function
V^*	Maximum velocity function at $z = z^*$
w_o	normal component of a gust velocity on the blade
x, y, z	blade fixed coordinate in aerodynamics
x_i	space fixed coordinate in acoustics
x_o	initial distance from the vortex core to the leading edge of the following blade
y_i	blade fixed coordinate in acoustics
z	r/r_t
z^*	r^*/r_t
Γ	circulation on the blade tip or circulation in vortex core
Γ_m	maximum circulation on the blade tip
Γ_1	maximum circulation on the vortex $\simeq \Gamma_m$
$\delta( )$	delta function
Δt	delayed reception time due to the span length
ϵ	eddy viscosity $k^2(r/\rho)^{\frac{1}{2}} r$
∇	gradient $(\frac{\partial}{\partial_x}, \frac{\partial}{\partial_y}, \frac{\partial}{\partial_z})$
μ	absolute viscosity
ν	kinematic viscosity μ/ρ
ρ	air density
ρ_o	air density in the medium at rest
ρ_t	signal width/period
σ	time at the leading edge during the interaction
ϕ	disturbed potential function
ω	angular frequency
Ω	helicopter rotor angular speed
$\psi(s)$	Küssner function
τ	emission (or retarded time) for moving source or circumferential shear stress

*Graduate Student, Student Member AIAA
+Director, Fellow AIAA

1. INTRODUCTION

One of the primary sources of noise for a helicopter, under certain flight conditions, arises from the interaction of the vortex produced by a blade with the aerodynamics of the following blade. To analyze this impulsive noise, sometimes called "blade slap," three parts of

the phenomena must be considered; the tip vortex generated by the blade, the unsteady pressure produced on the following blade during the interaction, and the acoustic radiation due to this unsteady pressure field.

This phenomena was first studied by Leverton and Taylor[1] experimentally using a rotating blade and two opposed airjets to simulate the tangential velocity profile of the vortex. Using the theory[2] of nonuniform flow past a thin airfoil, Sears[3] treated the line vortex as a gust; the vortex is forced to move parallel to the blade span with a displacement of half of the chord height. Parthasarathy and Karamcheti[4] solved this problem with a free point vortex, whose path is disturbed by the blade during the interaction from the intial height of half chord, and they calculated the quadrupole effect corresponding to the acoustic sources in the flow fields. Widnall,[5] who formulated an acoustic model for an oblique forced vortex using the quasi 2-D unsteady aerodynamics obtained by Johnson[6] and Filotas,[7] extended the theory to study the blade tip loading shape effect[8] and the high speed effect[9]. The Betz inviscid vortex model[10] was used to relate the tip loading shape and the viscous core was treated by using an effective distance between the center of the vortex and the blade. A number of researchers[11,12,13] have recently studied transonic effects on the unsteady aerodynamics due to the induced velocity of the vortex and others[14] have tried to predict the noise of the rotating blade using the measured aerodynamic pressure[15] on the blade surface.

In this paper, we attempt to study the effect of the turbulent viscous vortex core on the unsteady loading and acoustic pressure for the case of a close encounter with a following blade in certain flight condition as shown in Fig.1a. To analyze this phenomena, a simple analytical model of the vortex core, which is turbulent and viscous, is obtained by relating it to the tip aerodynamic parameters and we assume that the interactions occur in the persistent region of the vortex. To simplify the problem, we consider the situation where the vortex filament generated from the rotating tip is aligned

(a) side view

(b) plan view

Fig. 1. Trajectories of rotating tip vortex [4]

parallel to the following blade as shown in Fig.1b; in that situation the maximum acoustic pressure due to interaction is observed [16,17]. Even with the assumption of 2-D aerodynamics, the flow is too complicated to analyze completely as indicated in the experiment done by Ziada and Rockwell[18] so we assume that during the interaction the vortex path and vortex core are not distorted when cut by the following blade. Acoustic pressure is calculated for the finite unsteady source moving straight toward the fixed observer and analysed in the space fixed coordinate and reception time domain, whereas the source is described in the body fixed coordinate and emission time domain. Based on the analysis mentioned above, the trade-off of noise and performance is discussed.

2. ANALYSIS

2.1. ROTOR TIP VORTEX

It is observed that the rotor tip vortex quickly rolls into a concentrated vortex and persists for many span lengths before it decays (as in the case of the fixed wing tip vortex). However, because of the unsymmetric circulation shape toward the tip and the unrolled inboard vortex sheet of a rotor blade, the rotor vortex is more complicated to describe. Thus, for simplicity the rotor vortex field is modelled as a vortex pair, i.e., a tip vortex with an equivalent counter vortex of the same strength , which replaces the unrolled inboard vortex sheet. The curvature of the vortex filament is neglected locally during the formation and the oncoming velocity near the tip is assumed equal to the velocity at the position of the maximum circulation on the span. With this tip vortex model, the vortex core structure and strength are related with the tip aerodynamic parameters and are determined by following the general approach used by Spreiter-Sacks[18] for the potential part and by Roberts,[19] , for the turbulent viscous core.

Relation between tip aerodynamic parameters and vortex core

Consider a rotor blade of radius, R, rotating with an angular velocity Ω in a stream of uniform velocity U_∞. The blade will have a point of maximum circulation at a radial distance R_m. With the assumption of an equivalent tip vortex, it is convenient to consider the lift and drag on the rotor outboard of the radius R_m. Thus

$$L_{tip} = \frac{1}{2}\rho(\Omega R_m)^2 C_{Lt} A_t \qquad (1)$$

Generally, the lift coefficient C_{Lt} and equivalent tip area A_t are the functions of azimuthal angle ψ. The lift can be expressed, alternatively, as the integral of the distribution of circulation around the blade as

$$L_{tip} = \rho(\Omega R_m) \cdot 2(R - R_m)\Gamma_m \int_0^1 Gd(\frac{y}{R - R_m}) \qquad (2)$$

where Γ_m is the circulation at R_m, and $G = \Gamma/\Gamma_m$ as shown in Fig.2. Then, from (1) and (2),

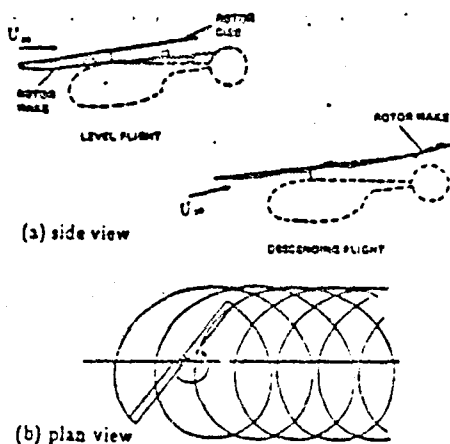$$\Gamma_m = (\Omega R_m)(R - R_m)\frac{C_{Lt}}{A R_t}\frac{1}{s_t} \qquad (3)$$
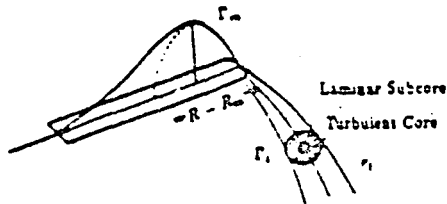
Fig. 2. Relation between the spanwise circulation and tip vortex

where

$$s_t = \int_0^1 G d\left(\frac{y}{R - R_m}\right) \qquad (4)$$

The quantity s_t represents the load characteristic of the tip and AR_t is the equivalent aspect ratio with equivalent span length of $2 \cdot (R - R_m)$.

It is well known that a size of the rolled up vortex is related to the lift-induced drag and is determined by the integration, in the plane normal to the axis of the vortex, of the rate of formation of rotational kinetic energy, as was used by Spreiter[18] i.e.

$$D_{it} = \int\int_{pot.} \frac{1}{2}\rho(v^2 + w^2)dS + 2\int_0^{r_1} \frac{1}{2}\rho v_\theta^2 2\pi r dr \qquad (5)$$

where

$$D_{it} = \frac{1}{2}\rho(\Omega R_m)^2 C_{D_{it}} A_t \qquad (6)$$

and

$$v_\theta = \frac{\Gamma}{2\pi r} \qquad (7)$$

The rotational energy has two parts; one from the potential part of the two point vorticies outside of the equivalent tip vortices and the other from the vortex cores of radius r_1. The vortex core structure is assumed not affected by the vortex pair, so it becomes a circular flow and its circulation Γ is a function of the radial distance r. The strength of the point vortex, Γ_t is assumed the same as the maximum circulation on the blade, Γ_m, which is actually almost 90% of Γ_m in the experiment data of Tung[20].

By combining Equation (2) and (7), Equation (5) can be expressed as below after integration of the potential part.

$$\frac{4s_t^2}{e_t} = \sinh^{-1}\left(\frac{r_d}{r_1}\right) + \int_0^{r_1}\left(\frac{\Gamma}{\Gamma_t}\right)^2 \frac{dr}{r} \qquad (8)$$

where the quantity e_t is the tip aerodynamic efficiency defined as

$$e_t = \frac{C_{L_t}^2}{\pi AR_t C_{D_{it}}} \qquad (9)$$

and r_d is half of the separation distance between the vortex pair determined by using the conservation of centroid of the vorticity

$$r_d = (R - R_m)\int_0^1 y\frac{dG}{dy}dy = (R - R_m)s_t \qquad (10)$$

Then r_1, the radius of the turbulent vortex core, may be expressed in closed form as shown below

$$r_1 = (R - R_m)s_t\left[\sinh\left(\frac{4s_t^2}{e_t} - \frac{11}{12}\right)\right]^{-1} \qquad (11)$$

The rotational energy of the core is obtained from the G in equation (16), which will be discussed in the following section.

The turbulent viscous vortex core

For large distances from the vortex center, the tip vortex behaves like a point vortex of constant strength Γ_t. Near the center of the vortex, where the turbulent and viscous effects are significant, the vortex core can be described by a differential equation expressing the transport of angular momentum, $2\pi r v_\theta$, in body fixed cylindrical coordinate (r, θ, z), as shown in Fig.3. Assuming the axial gradient is smaller than the radial gradient, the equation is written

$$u\frac{\partial G}{\partial z} + v\frac{\partial G}{\partial r} = r\frac{\partial}{\partial r}\{(\nu + \epsilon)\frac{1}{r}\frac{\partial G}{\partial r}\} \qquad (12)$$

where u is the axial velocity and v is the radial velocity, and ν, ϵ are the kinematic and eddy viscosity, respectively. The eddy viscosity for vortical flow has been analyzed by Hoffman and Joubert[21] in a way analagous to the traditional mixing length theory of Prandtl :

$$\epsilon = k^2(\tau/\rho)^{\frac{1}{2}}r \qquad (13)$$

where

$$\tau/\rho = \frac{\epsilon}{r}\frac{\partial}{\partial r}(rv_\theta) \qquad (14)$$

($k \approx 0.06$ appears to fit the experimental data[22] at a distance, d where the vortex starts decaying).

In the axial direction, there is an axial velocity defect in the core due to the viscosity such that the mean velocity in the plane normal to the axial direction is zero at the trailing edge. It is assumed here that the axial velocity varies linearly from the trailing edge to a distance, d, where the vortex starts decaying. Then, the inward radial velocity v is determined from the continuity equation. This inflow into the center balances the viscous and turbulent diffusion such that a persistent region of the tip vortex exists.

With the velocity components u, v assumed and eddy viscosity formulated in equation (13), a similarity solution for G was obtained by Roberts[18] with the boundary conditions that the tangential velocity, v_θ at the center is zero and the core merges with the potential flow. The tangential velocity of the vortex can be
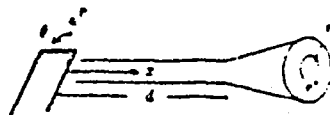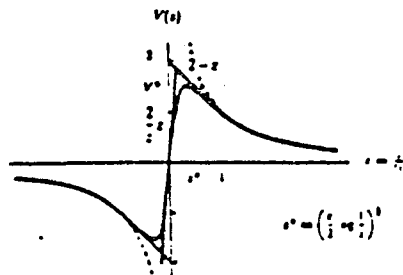

Fig. 3. Tip vortex geometry

Fig. 4. Vortex velocity distribution

expressed as follows :

$$v_\theta = \frac{\Gamma_1}{2\pi r_1(z)} V(z) \qquad (15)$$

where

$$V(z) = G(z)/z$$
$$= \left[1 - (1 - z^2)\left(1 + \frac{2z}{c}\right)' \right]/z \qquad z \leq 1 \quad (16)$$
$$= 1/z \qquad z \geq 1$$

The similarity variable, z, is defined as $r/r_1(z)$, where the turbulent core radius r_1 remains constant and equal to $r_1(0)$ for $z \leq d$ and increases as $r_1(0)\sqrt{z/d}$ for $r \geq d$. The persistence distance, d is $\pi/4k^2(\Omega R_\infty r_1^2(0)/\Gamma_1)$. The velocity function $V(z)$ of equation (16) is valid for small c ,which is a nondimensional parameter related to the inverse to the Reynolds Number, Re, defined as

$$c = \frac{2\pi\nu}{k^2\Gamma_1} = \frac{2\pi}{k^2}\frac{1}{Re} \qquad (17)$$

where Re, based on the maximum circulation Γ_1 in the vortex, is related to the blade chord length as a characteristic length :

$$Re = \frac{\Omega R_\infty}{\nu}\frac{2(R - R_\infty)}{AR_t}\cdot\frac{C_{Lt}}{s_t} = \frac{\Gamma_1}{\nu} \qquad (18)$$

(for a typical model rotor blade $c \sim 0.01$ to 0.1 and $Re \sim 10^4$ to 10^5).

The velocity function $V(z)$ can be expressed in a simple form as shown in Fig. 4. :

$$V(z) = \frac{2}{c}z \qquad \text{for the laminar sub core}$$
$$V(z) = 2 - z \qquad \text{for the turbulent core} \qquad (19)$$

The maximum velocity $V^* = 2 - 2z^*$ occurs at the position $z^* = (c/2 \ \log 1/c)^{1/2}$ as shown in Fig.4 and the velocity profile near the center,in the laminar sub core, shows that the velocity gradient is steeper for smaller value of c; that is, for large Re, which property becomes important for close encounters of the vortex with a following blade.

2.2. UNSTEADY AERODYNAMICS DURING THE INTERACTION

'With the tip vortex defined in the previous section, the unsteady flow field during the interaction between the vortex core and the following blade will be described with the assumption of no distortion of the vortex path or of the vortex core. Even though the vortex is turbulent and viscous, it is assumed that the flow around the airfoil is a potential flow during the interaction. These assumptions mean that the vortex is forced, not free, and the vorticity field of the vortex core and the irrotational field around the blade can be split and coupled through the surface boundary of the blade as explained more generally by Kovásznay[23] and Goldstein[24]; this is the same assumption as for traditional gust theory. Thus the vortex behaves like a convecting wave. These concepts were visualized by Rogler[23] in the problem of the interaction of a vortex array, representing the turbulent flow, with a semi-infinite plate. It shows that the stream function representing the vortical fields is not distorted but the combined stream function including the disturbed irrotational fields, satisfying the boundary condition of no flow through the solid boundary, is distorted to give a vortex on either side of the plate. This flow pattern is in general agreement with the experiments of Yu[26] in the extreme case for which the center of the vortex core meets the blade. Within these assumptions, only the normal component of the vortex velocity on the blade surface is important especially in case of no angle of attack between the convecting flow and blade. Even though the assumptions are valid only when the normal component of the velocity is small compared to the convecting velocity, we use the assumptions generally to derive the unsteady loading on the blade surface during the interaction.

Unsteady loading on the surface

The governing equation for the incompressible small perturbation potential fuction, ϕ, is

$$\nabla^2\phi = 0 \qquad (20)$$

and the boundary conditions are

$$\frac{\partial\phi}{\partial z} = -w_s(z - U\tau) \qquad |z| \leq b \quad z = 0$$
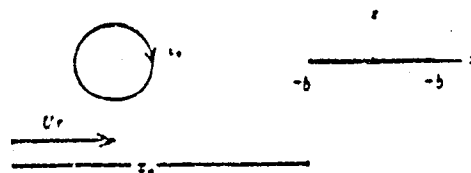$$p = 0 \qquad |z| \geq b \quad z = 0 \qquad (21)$$

Fig. 5. Coordinate system of the blade during interaction

where w_g is the normal component of the vortex gust. The pressure is given by the Bernoulli equation

$$p = -\rho_o \left(\frac{\partial \phi}{\partial \tau} + U \frac{\partial \phi}{\partial x} \right) \qquad (22)$$

Using the conservation of circulation in the flow field and the Kutta condition at the trailing edge, the lift for a sharp-edged gust was obtained by Küssner[27], (with the assumption that the shedding vorticies from the trailing edge covect with the same velocity of the free stream), as

$$L(s) = 2\pi\rho_o U b w_g \psi(s) \qquad (23)$$

where w_g = constant and

$$\psi(s) = \frac{1}{2\pi} \int_{-\infty}^{\infty} \frac{[C(k)][J_0(k) - iJ_1(k)] - J_1(k)]e^{ik(s-1)}}{ik} dk \qquad (24)$$

and

$$s = \frac{U\tau}{b}, \qquad k = \frac{\omega b}{U} \qquad (25)$$

The variable s is nondimensionalized time and k is the reduced frequency. The function $\psi(s)$ is the lift response function for the step gust, called the Küssner function.

For the vortex gust, we can use the Duhamel theorem to obtain the lift using the Küssner function. Thus,

$$L(s) = 2\pi\rho_o U b \left[w_g(0)\psi(s) + \int_0^s \frac{dw_g(\sigma)}{d\sigma}\psi(s-\sigma)d\sigma \right] \qquad (26)$$

Here, the velocity of the vortex gust w_g is obtained after the transformation of the coordinates as shown in Fig.5 :

$$w_g = \frac{\Gamma_1}{2\pi r_1} V \left(\frac{x_o - \sigma b}{r_1} \right) \qquad (27)$$

and the gradient of the gust velocity is

$$\frac{dw_g(\sigma)}{d\sigma} = -\frac{\Gamma_1}{2\pi r_1} \cdot \frac{b}{r_1} V'(\frac{x_o - \sigma b}{r_1}) \qquad (28)$$

where the quantity at time σ is of the convecting vortex velocity at the leading edge and x_o is the initial distance between the center of the vortex and the leading edge. As shown in Fig.6, the gradient of the gust velocity depends on the turbulent vortex size, r_1, the laminar sub core radius, r^* and the slope at the center of the c. $2/c$. The lift can be evaluated easily analytically or numerically if the Küssner function, which has the integration for the whole range of frequency as shown in equation (24), can be approximated in a simple analytical form.
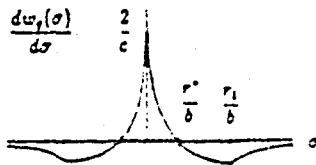
Fig. 6. Profile of the convecting vortex velocity gradient at the leading edge (center shifted by x_o/b)

Behavior of the Küssner function

The approximate form of the Küssner function can be expressed in a series of exponential terms as[28] is

$$\psi(s) = 1 - 0.5e^{-0.13s} - 0.5e^{-s} \qquad s \geq 2 \qquad (29)$$

This is valid for the whole range of s except near the origin where a more accurate form can be obtained by using the asymtotic expression of the function near the origin, $s \leq 2$, (the time required for the front of the step gust to pass over the chord), as follows

$$\psi(s) = \frac{\sqrt{2s}}{\pi} \left(1 - \frac{s}{12} + \frac{s^2}{96} - \frac{23}{13440}s^3 \right) \qquad s \leq 2 \quad (30)$$

Comparing (29) and (30), there is no significant difference in the unsteady loading as shown in Fig.7 . But if this loading acts as the acoustic source, a significant difference occurs near the origin because it involves the gradient of the function. Then for $s \leq 2$,

$$\frac{\partial\psi(s)}{\partial s} = \frac{\sqrt{2s}}{\pi} \left(\frac{1}{2}\frac{1}{s} - \frac{3}{2}\frac{1}{12} + \frac{5}{2}\frac{1}{96}s - \frac{7}{2}\frac{23}{13440}s^2 \right) \quad (31)$$

and for $s \geq 2$,

$$\frac{\partial\psi(s)}{\partial s} = 0.5 \cdot 0.13e^{-0.13(s+0.31)} + 0.5e^{-(s+0.31)} \qquad (32)$$

The gradient of the function has an integrable singularity at the origin and the exponential terms are modified to give a smooth function at $s = 2$. This is shown in Fig.8 .
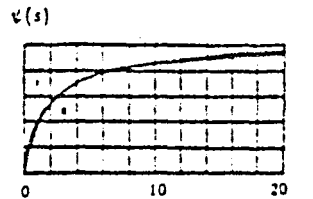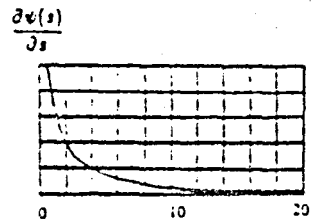

Fig. 7. Küssner function

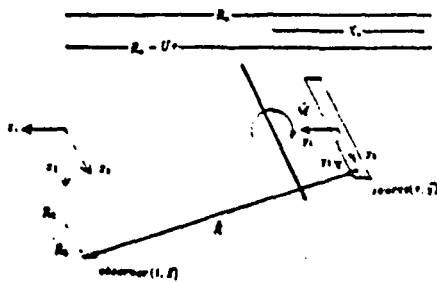Fig. 8. Gradient of the Küssner function

Fig. 9. Coordinate of the moving source

2.3. ACOUSTIC PRESSURE

The acoustic pressure field for a moving body in the presence of a vortex can be obtained by using the Ffowcs-Williams and Hawkings equation[29] in the medium at rest and by assuming the nonuniformity is confined to the sources. The signal is analyzed in space fixed coordinates and the sources are described in body fixed coordinates. The equation has monopole, dipole and quadrupole sources corresponding to thickness, surface pressure and unsteady flow fields. Here we consider only the dipole source because, assuming a thin airfoil and low mach number, we can neglect the monopole and quadrupole terms. As explained by Curle[30], the dipole source in the equation implies the effect of scattering due to the body for wave lengths of the signal large compared with the body size; then the source can be represented by the total force on the surface. Actually the observed acoustic signature during the blade vortex interaction contains all frequencies[31] but considering that most of the energy comes from the lower frequencies, a compact source can give the basic property of the signal. Here, in our problem of a finite source with large AR, a spanwise noncompact source is assumed.

The inhomogeneous wave equation with a moving dipole source is

$$\left(\frac{\partial^2}{\partial t^2} - a_o^2 \nabla^2\right)(\rho - \rho_o) = -\frac{\partial}{\partial x_i}\left(p_{ij}\delta(f)\frac{\partial f}{\partial x_j}\right) \quad (33)$$

where a_o is the speed of sound in the medium at rest and p_{ij} is the compressed stress, and f is a function of the body surface.

The solution in 3-D space is

$$p(\vec{x}, t) = -\frac{1}{4\pi}\frac{\partial}{\partial x_i}\int_S \left[\frac{p_{ij}n_j}{R\,|\,1 - \vec{M}\cdot\frac{d}{R}\,|}\right]_{r_e} dS(\vec{y}) \quad (34)$$

where $p = a_o^2(\rho - \rho_o)$ and $R = |\vec{x} - \vec{y}U r_e - \vec{y}|$ as shown in Fig.9. The source is evaluated in emission time r_e. The time relation

$$r_e = t - \frac{R(r_e, \vec{y})}{a_o} \quad (35)$$

is related to the Doppler shift because of the moving

source and

$$1/|\,1 - \vec{M}\cdot\vec{R}/R\,| \quad (36)$$

is the Doppler factor in amplitude.

Far field approximation

For the far field, the solution can be expressed in terms of a time derivative instead of a space derivative and for a chordwise compact but spanwise noncompact source, it can be written as follows (after using the relation of (35))

$$p(\vec{x}, t) = -\frac{1}{4\pi a_o}\frac{R_i^*}{R^{*2}\,|\,1 - \vec{M}\cdot\frac{d_i^*}{R^*}\,|^2} \int_{-l_o}^{+l_o}\left[\frac{\partial}{\partial r}L(r, y_3)\right]_{r_e} dy_3 \quad (37)$$

where R^* is the distance from the observer to the center of the source. For rectilinear moving source, the emission time is obtained as shown below

$$r_e = \frac{t - \frac{R_o M}{a_o}}{1 - M^2}$$
$$\mp \frac{\sqrt{\left(t - \frac{R_o M}{a_o}\right)^2 - (1 - M^2)\left\{t^2 - \frac{R_1^2 + R_2^2 + (R_3 - y_3)^2}{a_o^2}\right\}}}{1 - M^2} \quad (38)$$

The acoustic pressure is composed of two parts; the directivity function of the point source and integration of the source along the span. The integrand of the time variation of the lift can be obtained as shown below using the Duhamel integration of the gradient of the Küssner function, defined in (31) and (32), which represents the acoustic response function for the step gust,

$$\frac{\partial L}{\partial s}(s, y_3) = 2\pi \rho_o Ub \cdot \left[w_s(0)\frac{\partial \psi(s)}{\partial s} + \int_0^s \frac{dw_s(\sigma, y_3)}{d\sigma}\frac{\partial \psi(s - \sigma)}{\partial s}d\sigma\right] \quad (39)$$

The acoustic pressure also depends on the gradient of the gust which is function of r_t and c as shown in Fig.6. The schematic diagram for the Duhamel integration is shown in Fig.10, where the contribution of the gradient of the center of the core is large because of the delta-function-like acoustic response function. The contribution to the integral along the span of equation (37) comes from two factors: one from the lift variation along the span, which is zero in our 2-D aerodynamics, and the other from the emission time variation along the span as seen in equation (38).
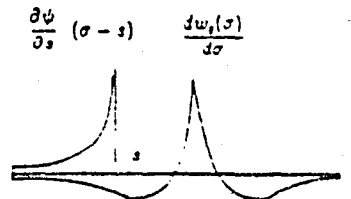

Fig. 10. Schematic diagram of the Duhamel's integration

An alternative form of the integral in equation (37) can be obtained by changing the variable of integration y_3 to τ as shown below

$$p(\bar{z},t) \sim \int_{\tau-(t-t_0)}^{\tau+(t-t_0)} \frac{\partial}{\partial \tau} L(\tau) \cdot \frac{\partial y_3(t,\tau)}{\partial \tau} d\tau \qquad (40)$$

Then, from the relation of the variables y_3 and τ in (38),

$$p \sim \int_{s_-}^{s^+} \frac{\partial L(s)}{\partial s} \frac{\{(1-M^2)s - \bar{t} - \overline{R}_o M^2\}}{M\sqrt{(\bar{t}-s)^2 - M^2((\overline{R}_o - s)^2 + \overline{R}_t^2)}} ds \qquad (41)$$

where the quantities $\overline{R}_o$ and $\overline{R}_t$ are the nondimensionalised distances by the semichord length b and $\bar{t}$ is the nodimensionalised reception time by b/U as s in (25). This form is useful in evaluation of the integral because the integrand is the direct function of the variable of integration, s.

Interference of the spanwise non-compact source

The integral of the spanwise noncompact source can be interpreted as the interference between multiple point source signals. Then $\partial L(s)/\partial s$ can be expressed in the emission time domain with measured or computed values of $L(s)$ for each span location. Each signal is transformed to the reception time domain as shown in Fig.11(b) with the time relation $t = \tau_e + R(\tau_e, y_3)/a_o$. The amplitude is the same for corresponding t and τ. Then each signal is summed in the reception time domain as shown in Fig.11(c) . The delayed time (in the reception time domain) due to the different source positions causes the interference, which contributes to the amplitude in a destructive way and also to the directivity pattern in addition to the point source directivity.

The interference is closely related to the ratio of Δt and d_t (nondimensionalized by b/U), where the width of the signal, d_t depends on the position of the maximum velocity of the vortex and the maximum delayed time along the span, Δt depends on the observer position, as shown in Fig.12. If the observer is far from the plane of symmetry of the source, greater interference is
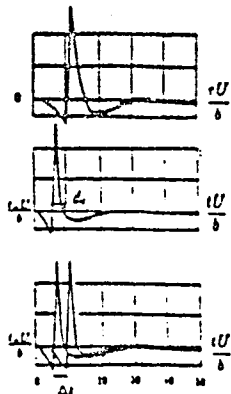
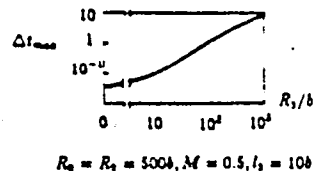Fig. 11. Interference process of the spanwise noncompact source

$R_o = R_t = 500b, M = 0.5, t_3 = 10b$

Fig. 12. Variation of delayed signal time with observer position
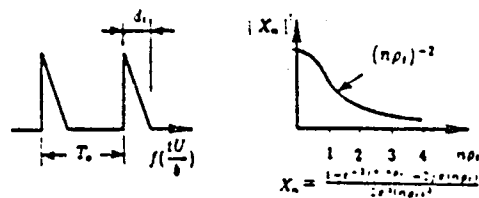

$$X_n = \frac{1 - r^{1/r} \cdots}{\cdots}$$

Fig. 13. Simplified model signal in time domain and its spectrum

maximum acoustic pressure is observed; then the source can be approximated as a point source to evaluate the maximum acoustic pressure in this simple geometry .

The effective ratio of Δt and d_t can be estimated from a simplified point source signal and its spectrum as shown in Fig.13. Assuming that the spectrum begins to decay significantly at $n\rho_t = N$ where the the solidity ρ_t is defined as d_t/T_o, the corresponding angular frequency of nth$(= N/\rho_t)$ harmonic, ω_n is $2\pi n/(T_o b/U) = 2\pi N/(d_t b/U)$. Thus the reduced frequency, k_n is $\omega_n b/U = 2\pi N/d_t$ and the frequency, f_n is $\omega_n/2\pi = N/(d_t b/U)$, and the nondimensionalized period, T_n is $1/f_n$ $U/b = d_t/N$. From Fig.13, it is seen that for $N = 1$, then $T_n = d_t$, the contributions of the waves for which periods are less than d_t are small. So if the delayed time is greater than the period T_n (approximately, $\Delta t \geq d_t/4$), interference will occur.

3. RESULTS & DISCUSSIONS

From the previous analysis, we find that the unsteady lift and the acoustic pressure are closely related to the slope of the vortex velocity, which is the function of the vortex turbulent core size r_t and a nondimensional parameter c (inverse of Reynolds Number Re).
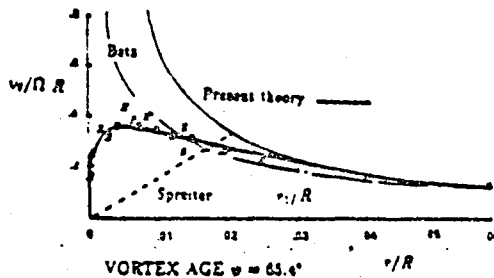
The vortex velocity profile is computed and compared with the experimental data obtained by Tung[20]. The unsteady lift and acoustic pressure are calculated and the variation of maximum acoustic pressure with the parameters r_t and c is examined. The noise/performance trade-off for blade tip loading shape is also discussed.
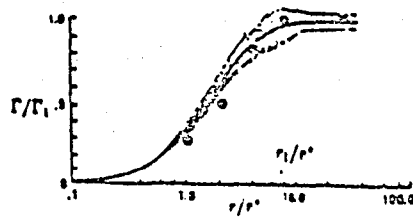
Vortex Velocity Profile

The vortex structure generated by a blade having radius $R = 1.05m$ and aspect ratio $AR = 13.7$, are computed. The general structure shows good agreement with experiment even though the maximum velocity and its position are underpredicted as shown in Fig. 14. The velocity profile predicted with our analysis is compared with that predicted with Betz analysis for the persistence region. Both show generally good agreement outside of the core but within the core the present analysis is more realistic since the Betz vortex has infinite velocity especially for the elliptic tip loading. In both cases, the distance from the location of the maximum circulation to the tip is taken to be 5% of the blade span length. It should be mentioned that the maximum rotational velocity of the vortex is almost 40% of the rotating tip speed in this case. But if the position of maximum circulation is shifted toward the root, the maximum velocity of the vortex is reduced substantially.

Unsteady Lift and Acoustic Signal

Typical nondimensional unsteady lift and acoustic pressure for the vortex gust are plotted in Fig.15. It

(a) velocity profile

(b) circulation profile

Fig. 14. Vortex core velocity profile comparision
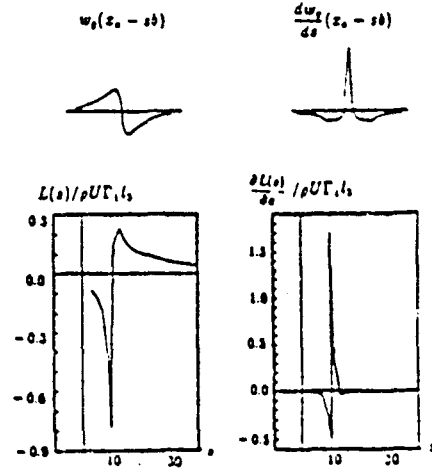
Fig. 15. Typical variation of unsteady lift and acoustic signal

is observed that the lift profile is similar to the vortex velocity profile but distorted due to the behavior of the Küssner function which introduces a time lag near the origin. The acoustic signal, in the emission time domain, is similar to the slope of the vortex velocity profile because the acoustic function acts like a delta function which assumes the value of the slope during the integration. So the amplitude of the peak acoustic pressure is related to the slope of the vortex at the center of the laminar sub core, $2/c$ and the width of the signal is related to the radius of the laminar core, r^*.

Reynolds Number and Vortex Size Effect

It is to be expected that both the peak unsteady lift and the acoustic pressure decrease with larger turbulent vortex core size r_t and smaller Reynolds Number($Re = \Gamma_t/\nu$) because the gust function is $\Gamma_t/2\pi r_t \cdot V(\sigma/r_t)$. But the acoustic pressure is more sensitive to the slope of the core($Re \sim 2/c$) shown in Fig.6, because again the behavior of the delta function like the acoustic function varies as the slope of the laminar core, $2/c$. For the maximum acoustic pressure, the effects of the Reynolds Number and vortex size are shown in Fig.16. To reduce this peak pressure, it is obvious that we need to reduce the vortex size r_t and Reynolds number Re. One method would be to increase the distance, $(R - R_m)$ between the location of the maximum circulation and tip, because r_t and Re both are directly related to it from the equation (11) and (18). But this would result in a loss of lift near the tip which is proportial to $(\Omega R_m)^2$ with the same lift coefficient. The other method would be to change the tip loading shape which is related to r_t for the fixed value of $(R - R_m)$ and Γ_t.
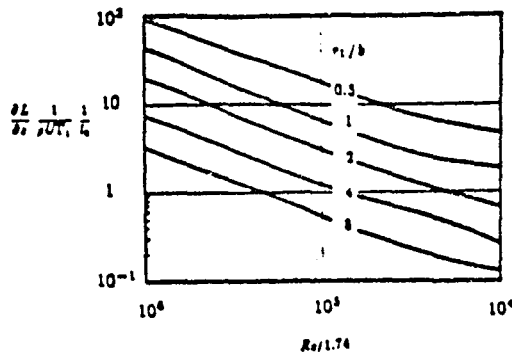
Fig. 16. Effects of Reynolds Number Re and vortex size r_{1}, on maximum acoustic pressure

Fig. 18. Trade off between noise reduction and aerodynamic efficiency for various m.

Noise Performance Trade-Off

The influence of blade loading on the noise and performance has been studied. The variations of the circulation shape of the form $\Gamma/\Gamma_1 = (\sin\theta)^{2m-1}$, where $\cos\theta = y/(R - R_m)$, are considered as shown in Fig.18(a)($m = 1$ is elliptic loading). For large value of m, the core radius increases and there is a reduction of noise compared with the elliptic loading, but the tip loading relief also gives a reduction in the tip aerodynamic efficiency defined in Equation (9) as shown in Fig.18(b). From Fig.19, a maximum noise reduction $5dB$ is obtained for $m = 2$ with 25% loss of efficiency and a noise reduction of $3dB$ with 5% loss of efficiency. For the triangular loading there is more than $8dB$ reduction in noise but also more than 30% reduction in efficiency.

Fig. 17. (a) Tip circulation profile (b) variation of $r_1/R - R_m$ and $\Delta p(dB)$ with tip-loading parameter m (c) Variation of tip efficiency with tip-loading parameter m

4. CONCLUSIONS

The blade vortex interaction where the turbulent viscous core is cut through by the blade is analyzed with the assumptions of no distortion of the vortex path and or vorticity of the core during the interaction. From the analysis and results, the following conclusions can be drawn :

(1) The detailed vortex structure including the viscous and turbulent core generated by the rotor tip can be approximately predicted with a simple turbulent core model and equivalent tip model.

(2) The interaction between the vortex core and the blade is analyzed with the gust analogy under the assumptions of no distortions of the vortex for the extreme case where the center of the core is cut through the vortex.

(3) Acoustic pressure is obtained by introducing the acoustic response function for the step gust for the chordwise compact source. It shows that the spanwise non-compact source gives a sizable effect when the observer is off-center of the source because of the large interference effect.

(4) Maximum acoustic pressure varies with Reynolds Number and vortex size, which are related to the tip loading.

(5) Shape modification gives a maximum reduction of $6 \sim 8dB$ including the triangular loading, but a reduction of $3dB$ in maximum acoustic pressure compared with the elliptic loading, is expected for 5% loss in efficiency.

For the extreme case of cutting through the core by the blade, the chordwise non-compact source should be considered in order to obtain results over the range of frequencies in the high speed case. It should mentioned that the non-linearity due to the large maximum vortex velocity and due to the quadrupole for this case, which would be the same order of the dipole, should be considered also.

REFERENCES

1. Leverton, J. W. and F. W. Taylor. "Helicopter Blade Slap", *Journal of Sound and Vibration* 4, No. 3, (1966), 345-357.

2. Sears, W. R., "Operational Methods in the Theory of Airfoils in Non-Uniform Motion", *Journal of the Franklin Institute* Vol. 230, 95-111, July 1940.

3. Sears, W. R., "Aerodynamics, Noise and the Sonic Boom", 1968 von Karman Lecture, *AIAA Journal*, 7, No. 4, April 1969.

4. Parthasarathy, "Aerodynamic Sound Generation due to Vortex-Aerofoil Interaction", Ph.D. thesis, Stanford University, Stanford, CA, September 1972.

5. Widnall, E. S., "Helicopter Noise due to Blade-Vortex Interaction", *Journal of the Acoustic Society of America*, 50, No. 1 (part 2) (1971), 354-366.

6. Johnson, W., "A Lifting Surface Solution for Vortex Induced Airloads and Its Application to Rotary Wing", MIT ASRL TR 153-2, April 1970.

7. Filatos, L. T. ,"Theory of Airfoil Response in a Gusty Atmosphere-Part 1 Aerodynamic Transfer Function", Inst. for Aerospace Studies, Univ. of Toronto UTIAS No. 139, October 1969.

8. Widnall, E. S. and T. L. Wolf, "Effect of Tip Vortex Structure on Helicopter Noise Due to Blade-Vortex Interaction", *Journal of Aircraft*, 17 (1980), 705-711.

9. Martinez, R. and E. S. Widnall, "An Aeroacoustic Model for High- Speed, Unsteady Blade-Vortex Interaction", *AIAA Journal* 21, No. 9, September 1983.

10. Betz, A., "Behavior of Vortex systems", NACA TM No. 713, June 1933.

11. George, A. R. and S. B. Chang, "Noise Due to Transonic Blade-Vortex Interactions", American Helicopter Society A-83-39-50-D000, May 1983.

12. McCroskey, W. J. and P. M. Goorjian, "Interactions of Airfoils With Gusts and Concentrated Vortices in Unsteady Transonic Flow", AIAA 16th Fluid and Plasma Dynamics Conference, Danvers, MA, July 1983.

13. Sirinivanson, G. R., W. J. McCroskey, and P. Kutler, "Numerical Simulation of the Interaction of a Vortex With Stationary Airfoil in Transonic Flow", AIAA 22nd Aerospace Sciences Meeting, Reno, Nevada, AIAA 84-0254, January 1984.

14. Hakamura, Y., "Prediction of Blade-Vortex Interaction Noise From Measured Blade Pressure", 33rd Annual National Forum of the American Helicopter Society, Washington, D. C., Paper 77, 33-05, 1977.

15. Shockey, G. A., J. W. Williamson, and C. R. Cox, "Helicopter Aerodynamics and Structural Loads Survey", the 32nd Annual National V/STOL Form of the American Helicopter Society, Washington, D. C., No. 1060, May 1976.

16. Ziada, S. and D. Rockwell, "Vortex-Leading Edge Interaction", *Journal of Fluid Mechanics*, 118 (1982), 79-107.

17. Schmitz, F. H. and Y. H. Yu, "Helicopter Impulsive Noise: Theoretical and Experimental Status", International Symposium on Recent Advances in Aerodynamics and Aeroacoustics, Stanford University, Stanford, CA, August 1983.

18. Spreiter, J. R. and A. H. Sacks, "The Rolling Up of the Trailing Vortex Sheet and Its Effects on the Downwash Behind Wings", *Journal of the Aeronautical Sciences*, 18, No. 1 (1951), 21-32.

19. Roberts, Leonard, "On the Structure of the Turbulent Vortex", AGARD SP NO. 342.

20. Tung, C. L. Pucci, and X. Caradona, "The Structure of Trailing Vortices Generated by Model Rotor Blades", NASA TM 81316, USAAVRADCOM TR- 81-A-25, August 1981.

21. Hoffman, E. R. and Joubert, P. N. "Turbulent Line Vortices", *Journal of Fluid Mechanics*, 16 (1963), 395-411.

22. Ciffone, D. L., Orloff, K. L., "Far-Field Wake-Vortex Characteristics of Wings", *Journal of Aircraft*, 12, No. 5, May 1975, pp. 464-470.

23. Kovásznay, L. S. G., "Turbulence in Supersonic Flow", *Journal of the Aeronautical Sciences*, 20, (1953), 657-674.

24. Goldstein, M. E., "Aeroacoustics", McGraw Hill, 1976.

25. Roger, H., "The Interaction between Vortex Array Representations of Free-Stream, Turbulence and Semi-Infinite Flat Plates", *Journal of fluid Mechanics*, (1978), no. 583-606.

26. Küssner, H. G., "Zurammenfassender Bericht über den instationären Auftrieb von Flügelen", Luftfahrtforsh, Bd. 13, Nr. 12, December 1936.

27. Yu, J. C., "Flow-Field Visualisation of Two-Dimensional Blade-Vortex Encounters", Workshop on Blade-Vortex Interactions, Ames Research Center, Moffett Field, CA, October 1984.

28. Bisplinghoff, Ashley, and Halfman, Aero-Eelasticity, Addison-Wesley, 1955.

29. Ffowcs-Williams and Hawkings, " Sound Generation by Turbulence and Surfaces in Arbitrary Motion", Phil. Tran. Roy. Soc. Lon, Ser. A, 264 (1969), 321-342.

30. Curle, N.,"The Influence of Solid Boundaries upon Aerodynamic Sound", Proc. Roy. Soc. Lon. 231 A, (1955) 505-514.

31. Boxwell, D. A. and F. H. Schmitz, "Full-Scale Measurements of Blade-Vortex Interaction Noise",*Journal of the American Helicopter Society*, October 1982, pp.11-27

N85
25215

UNCLAS

Appendix C

FLOW PAST A FLAT PLAT WITH A VORTEX/SINK COMBINATION

Nikos J. Mourtos

ABSTRACT

An attempt has been made to model the so called "Leading Edge Vortex" which forms over the leading edge of delta wings at high angles of attack.

A simplified model has been considered, namely that of a two-dimensional, inviscid, incompressible steady flow around a flat plate at an angle of attack with a stationary vortex detached on top, as well as a sink to simulate the strong spanwise flow.

The results appear to agree qualitatively with experiments. A comparison has also been made between the lift and the drag of this model and the corresponding results for two classical solutions:

(i) that of totally attached flow over the plate with the Kutta condition satisfied at the trailing edge only.

(ii) the Helmholtz solution of totally separated flow over the plate.

NOMENCLATURE

English letter symbols:

a radius of the cylinder.

b length of the span of the plate.

c chord length of the plate.

C_D drag coefficient.

C_L lift coefficient.

C_M pitching moment coefficient.

C_P pressure coefficient.

d distance between the streamlines leading to the two stagnation points on the plate.

D drag force.

F total force on the plate.

k total vortex strength.

k_0 bound vortex strength.

k_1 leading edge vortex strength.

K non-dimensional total vortex strength.

K_0 non-dimensional bound vortex strength.

K_1 non-dimensional leading edge vortex strength.

L lift force.

$\dot{m}$ mass flow rate.

m_1 sink strength.

M_1 non-dimensional sink strength.

n non-dimensional parameter showing position along the plate.

r, θ polar coordinates in the z-plane.

R_1 non-dimensional distance from the center of the cylinder to equilibrium point.

S wing area.

u, v velocity components.

V_∞ free stream velocity.

w complex potential.

x, y cartesian coordinates in the z-plane.

z complex variable in the original circle plane.

$\bar{z}$ complex conjugate of z.

z' complex variable in the rotated circle plane.

Greek letter symbols:

α angle of attack.

Γ total circulation.

Γ_0 circulation due to the bound vortex.

ς complex variable in the final plate plane.

ς' complex variable in the Joukowski plane.

ξ, η coordinates in the ς-plane.

ξ', η' coordinates in the ς'-plane.

Λ_0 doublet strength.

ρ air density.

Subscripts:

c in the plane of the cylinder.

p in the plane of the plate.

r radial component.

sc on the surface of the cylinder.

sp on the surface of the plate.

TE at the trailing edge.

z in the z-plane.

θ tangential component.

ς in the ς-plane.

0 refers to the origin (center of the cylinder).

1 refers to the equilibrium point.

iii

TABLE OF CONTENTS

33

34

LIST OF FIGURES

1. INTRODUCTION

So far there are two well-known models for the flow over a flat plate at an angle of attack. That of totally attached flow with the Kutta condition satisfied at the trailing edge only, and that of totally separated flow (Helmholtz solution).

The present model, considering partially separated flow lies somewhere between the two and despite the fact that it too is two-dimensional, gives some very useful representation of the three-dimensional flow over delta wings. On such wings the leading edge is usually sharp, causing thus flow separations even at moderate angles of attack. These flow separations take the form of two free vortex layers joined to the leading edge of the wing and rolling up to form spiral shaped vertices above the upper surface of the wing (Figure 1a).

These vortices induce additional velocities at the upper surface of the wing. The corresponding pressure distribution shows distinctly marked minima beneath the vortex axes (Figure 1b). Accordingly, an additional lift force occurs which depends nonlinearly on the angle of attack (Figure 1c).

In the theoretical study made here, a simplified model has been considered, namely that of a two-dimensional, inviscid, incompressible steady flow over a flat plate at an angle of attack, with a stationary vortex detached on top as well as a sink to simulate the strong spanwise flow caused by the pressure gradient due to sweep in the three-dimensional case.

2. ANALYSIS OF THE FLOW FIELD

In the original circle plane (also called z-plane) the flow field consists of the following components:

(i) Uniform wind V_∞ coming from the negative x-axis.

(ii) A doublet A_0 at the origin to simulate a circular cylinder $|z| = a$.

(iii) A bound vortex k_0 at the origin to account for the circulation Γ_0 around the plate. Note that although the flow is aligned with the x-axis the plate is at an angle of attack, requiring thus circulation Γ_0 for the Kutta condition to be satisfied (see Figure 2a).

(iv) A steady vortex k_1 of finite radius placed at $z_1(r_1, \theta_1)$ to simulate the leading edge vortex.

(v) A steady vortex $-k_1$ at the inverse square point of z_1 induced by the circle theorem (see Appendix A1.1).

(vi) A steady vortex k_1 at the origin also induced by the circle theorem (see Appendix A1.1).

(vii) A sink m_1 ($m_1 < 0$) placed at $z_1(r_1, \theta_1)$ to simulate the spanwise flow along the center of the vortex.

(viii) A sink m_1 at the inverse square point of z_1, induced by the circle theorem (see Appendix A1.2).

(ix) A source $-m_1$ at the origin also induced by the circle theorem (see Appendix A1.2).

2.1 The Complex Potential

For the components described above (regrouping them together), the complex potential is given below:

$$w = V_\infty \left(z + \frac{a^2}{z} \right) + (-m_1 + ik) \ln z + (m_1 + ik_1) \ln(z - z_1) + (m_1 - ik_1) \ln \left(z - \frac{a^2}{\bar{z}_1} \right) \quad (1)$$

where

$$k = k_0 + k_1 \quad (2)$$

2

2.2 The velocity Field

Differentiation of the complex potential gives the velocity field:

$$\frac{dw}{dz} = (u_r - iu_\theta)\,e^{-i\theta} \tag{3}$$

which applied to equation (1) gives:

2.2.1 Radial Components

$$
\begin{aligned}
u_r = V_\infty \left(1 - \frac{a^2}{r^2}\right)\cos\theta - \frac{m_1}{r} &+ \frac{m_1[r - r_1\cos(\theta - \theta_1)] + k_1 r_1 \sin(\theta - \theta_1)}{r^2 + r_1^2 - 2rr_1\cos(\theta - \theta_1)} \\
&+ \frac{m_1 r_1[rr_1 - a^2\cos(\theta - \theta_1)] - k_1 r_1 a^2 \sin(\theta - \theta_1)}{r^2 r_1^2 + a^4 - 2rr_1 a^2 \cos(\theta - \theta_1)}
\end{aligned}
\tag{4}
$$

2.2.2 Tangential Components

$$
\begin{aligned}
u_\theta = -V_\infty \left(1 + \frac{a^2}{r^2}\right)\sin\theta - \frac{k}{r} &+ \frac{m_1 r_1 \sin(\theta - \theta_1) - k_1[r - r_1\cos(\theta - \theta_1)]}{r^2 + r_1^2 - 2rr_1\cos(\theta - \theta_1)} \\
&+ \frac{m_1 r_1 a^2 \sin(\theta - \theta_1) + k_1 r_1[rr_1 - a^2\cos(\theta - \theta_1)]}{r^2 r_1^2 + a^4 - 2rr_1 a^2 \cos(\theta - \theta_1)}
\end{aligned}
\tag{5}
$$

2.3 Conformal Transformation Used to Analyze the Flow Field

A solution for the flow field is provided by a mapping sequence that transforms the potential flow about a circle into a flow about a flat plate at an angle of attack with a detached vortex/sink combination. The steps are the following (see also Figure 2):

a. original circle plane (z-plane),

b. rotated circle plane (z'-plane), $z' = ze^{i\alpha}$,

c. Joukowski plane (ς'-plane), $\varsigma' = z' + \frac{a^2}{z'}$,

d. final plate plane (ς-plane), $\varsigma = \varsigma' e^{-i\alpha}$.

The first step is a simple rotation in order to make the flat plate depicted inside the circle aligned with the x-axis. The second step is the Joukowski transformation which transforms the circle into a flat plate. The third step is another rotation which gives the plate an angle of attack with respect to the horizontal free stream velocity.

Combining the three steps we have that

$$\varsigma = z + \frac{a^2}{z} e^{-2i\alpha} \tag{6}$$

or

$$z = \frac{\varsigma}{2} \pm \sqrt{\left(\frac{\varsigma}{2}\right)^2 - (ae^{-i\alpha})^2} \tag{7}$$

and if we set

$$\varsigma = \xi + i\eta \tag{8}$$

we get

$$\xi = r\cos\theta + \frac{a^2}{r}\cos(\theta + 2\alpha) \tag{9}$$

$$\eta = r\sin\theta - \frac{a^2}{r}\sin(\theta + 2\alpha) \tag{10}$$

On the surface of the cylinder (corresponding to the surface of the plate) $r = a$ so

$$\xi_{sp} = a\left[\cos\theta + \cos(\theta + 2\alpha)\right] \tag{11}$$

$$\eta_{sp} = a\left[\sin\theta - \sin(\theta + 2\alpha)\right] \tag{12}$$

now

$$\frac{dw}{d\varsigma} = \frac{dw}{dz} \cdot \frac{dz}{d\varsigma} \tag{13}$$

and

$$\frac{dz}{d\varsigma} = \frac{1}{d\varsigma/dz}$$

$$= \frac{z^2 e^{2i\alpha}}{z^2 e^{2i\alpha} - a^2}$$

$$= \frac{r^2 e^{i(2\alpha + 2\theta)}}{r^2 e^{i(2\alpha + 2\theta)} - a^2}$$

Considering the surface again ($r = a$), expanding the right-hand side into sines and cosines and using equation (3) we get finally

$$\left[u_{r_{sp}}\right]_\varsigma = \frac{\sin(4\theta + 4\alpha) - 2\sin(2\theta + 2\alpha) - 2\cos(2\theta + 2\alpha)}{2 + 2\cos(4\theta + 4\alpha) - 4\cos(2\theta + 2\alpha)} \cdot \left[u_{\theta_{ss}}\right]_z \tag{14}$$

$$\left[u_{\theta_{sp}}\right]_\varsigma = -\frac{1}{2\cos(2\theta + 2\alpha)}\left[u_{\theta_{ss}}\right]_z \tag{15}$$

4

3. CONDITIONS

Boundary conditions in the final plate plane require that:

(i) the flow depart smoothly from the trailing edge;

(ii) the flow depart smoothly from the leading edge, i.e., the Kutta condition must be satisfied at both edges of the plate.

Also, the vortex/sink combination must be located at an equilibrium point in the flow field, that is, a point where the velocity induced by all other components is zero.

3.1   Kutta Condition at the Trailing Edge

From equations (14) and (15) with $\theta = -\alpha$ we find the velocity components at the trailing edge of the plate:

$$\left[u_{r_{sp}}\right]_\zeta^{TE} = -\frac{1}{0}\left[u_{0_{ss}}\right]_z^{\theta=-\alpha} \tag{16}$$

$$\left[u_{r_{sp}}\right]_\zeta^{TE} = -\frac{1}{2}\left[u_{0_{ss}}\right]_z^{\theta=-\alpha} \tag{17}$$

For the Kutta condition to be satisfied there (i.e., u_r finite and $u_\theta = 0$) we must have

$$\left[u_{0_{ss}}\right]_z^{\theta=-\alpha} = 0 \tag{18}$$

or, from equation (5) with $r = a$ and $\theta = -\alpha$

$$\left(2V_\infty a\sin\alpha - k\right)\left[r_1^2 + a^2 - 2r_1 a\cos(\theta_1 + \alpha)\right] - 2m_1 r_1 a\sin(\theta_1 + \alpha) + k_1(r_1^2 - a^2) = 0 \tag{19}$$

3.2   Kutta Condition at the Leading Edge

Similarly, for the leading edge we must have

$$\left[u_{0_{ss}}\right]_z^{\theta=\pi-\alpha} = 0 \tag{20}$$

and again from equation (5) with $r = a$ and $\theta = \pi - \alpha$

$$\left(2V_\infty a\sin\alpha + k\right)\left[r_1^2 + a^2 + 2r_1 a\cos(\theta_1 + \alpha)\right] - 2m_1 r_1 a\sin(\theta_1 + \alpha) - k_1(r_1^2 - a^2) = 0 \tag{21}$$

3.3 Vortex/Sink Velocity Condition

Equation (3) cannot be used to find the conditions which make the velocity vanish at the location of the sink and vortex because the velocity given by equation (3) is singular there. Threfore, the usual limiting process has to be used to find the velocity components at the center of the vortex/sink combination. The strengths of the singularities can then be adjusted so that they are stationary in the presence of the plate. Following the analysis of reference 3 the complex velocity function in the final plate plane at the equilibrium point is found to be

$$[u_p - iv_p]_{\varsigma_1} = \left[(u_c - iv_c)\frac{dz}{d\varsigma} \right]_{z_1} - \frac{1}{2}(m_1 + ik_1)\frac{[d^2z/d\varsigma^2]_{\varsigma_1}}{[dz/d\varsigma]_{\varsigma_1}} = 0 \qquad (22)$$

The derivative $\frac{dz}{d\varsigma}$ has been found in Section 2.3:

$$\frac{dz}{d\varsigma} = \frac{(ze^{i\alpha})^2}{(ze^{i\alpha})^2 - a^2}$$

while

$$\frac{d^2z}{d\varsigma^2} = \frac{d}{d\varsigma}\left(\frac{dz}{d\varsigma}\right) = \frac{d}{d\varsigma}\left[\frac{z^2 e^{2i\alpha}}{z^2 e^{2i\alpha} - a^2} \right]$$

and substituting z from equation (7), taking the derivative and substituting back ς from equation (6) we get

$$\frac{d^2z}{d\varsigma^2} = \frac{a^2 e^{2i\alpha}[4z^4 + 3(z^2 + a^2 e^{-2i\alpha})^2]}{2z(a^2 e^{-2i\alpha} - z^2)(z^2 e^{2i\alpha} - a^2)^2}$$

Also, from Figure 3 we have the following transformations:

$$u_r = u_c \cos\theta + v_c \sin\theta$$

$$u_\theta = v_c \cos\theta - u_c \sin\theta$$

or

$$u_c = u_r \cos\theta - u_\theta \sin\theta$$

$$v_c = u_r \sin\theta + u_\theta \cos\theta$$

Substituting all these into equation (22) we get

$$[(u_{r1}\cos\theta_1 - u_{\theta 1}\sin\theta_1) - i(u_{r1}\sin\theta_1 + u_{\theta 1}\cos\theta_1)] z_1^2 e^{2i\alpha}$$

$$- (m_1 + ik_1)\frac{a^2 [4z_1^4 + 3(z_1^2 + a^2 e^{-2i\alpha})^2]}{2z_1(z_1^2 - a^2 e^{-2i\alpha})^2} = 0 \qquad (23)$$

6

where

$$z_1 = r_1 e^{i\theta_1} = r_1 \left(\cos\theta_1 + i\sin\theta_1\right) \tag{24}$$

Splitting into real and imaginary parts and substituting for u_{r1} and $u_{\theta 1}$ their equivalent expressions from equations (4) and (5) with $r = r_1$ and $\theta = \theta_1$ we get

$$2V_\infty r_1^5 (r_1^2 - a^2)^2 \cos\theta_1 \cos(6\theta_1 + 2\alpha) - 4V_\infty r_1^3 a^2 (r_1^2 - a^2)^2 \cos\theta_1 \cos 4\theta_1$$
$$+ 2V_\infty r_1 a^4 (r_1^2 - a^2)^2 \cos\theta_1 \cos(2\theta_1 - 2\alpha) - 2V_\infty r_1^5 (r_1^4 - a^4) \sin\theta_1 \sin(6\theta_1 + 2\alpha)$$
$$+ 4V_\infty r_1^3 a^2 (r_1^4 - a^4) \sin\theta_1 \sin 4\theta_1 - 2V_\infty r_1 a^4 (r_1^4 - a^4) \sin\theta_1 \sin(2\theta_1 - 2\alpha)$$
$$- 2k_0 r_1^6 (r_1^2 - a^2) \sin(6\theta_1 + 2\alpha) + 4k_0 r_1^4 a^2 (r_1^2 - a^2) \sin 4\theta_1$$
$$- 2k_0 r_1^2 a^4 (r_1^2 - a^2) \sin(2\theta_1 - 2\alpha) + 2k_1 r_1^6 a^2 \sin(6\theta_1 + 2\alpha)$$
$$+ k_1 r_1^4 a^2 (7r_1^2 - 11a^2) \sin 4\theta_1 + 7k_1 r_1^4 a^2 (r_1^2 - a^2) \cos 4\theta_1$$
$$+ 2k_1 r_1^2 a^4 (3r_1^2 - 2a^2) \sin(2\theta_1 - 2\alpha) + 6k_1 r_1^2 a^4 (r_1^2 - a^2) \cos(2\theta_1 - 2\alpha)$$
$$+ 3(k_1 - m_1)(r_1^2 - a^2)(\cos 4\alpha - \sin 4\alpha) a^6 + 2m_1 r_1^6 a^2 \cos(6\theta_1 + 2\alpha)$$
$$- m_1 r_1^4 a^2 (7r_1^2 - 3a^2) \cos 4\theta_1 - 7m_1 r_1^4 a^2 (r_1^2 - a^2) \sin 4\theta_1$$
$$- 2m_1 r_1^2 a^4 (3r_1^2 - 4a^2) \cos(2\theta_1 - 2\alpha) - 6m_1 r_1^2 a^4 (r_1^2 - a^2) \sin(2\theta_1 - 2\alpha) = 0 \tag{25}$$

ar.d

$$2V_\infty r_1^5 (r_1^2 - a^2)^2 \cos\theta_1 \sin(6\theta_1 + 2\alpha) - 4V_\infty r_1^3 a^2 (r_1^2 - a^2)^2 \cos\theta_1 \sin 4\theta_1$$
$$+ 2V_\infty r_1 a^4 (r_1^2 - a^2)^2 \cos\theta_1 \sin(2\theta_1 - 2\alpha) + 2V_\infty r_1^5 (r_1^4 - a^4) \sin\theta_1 \cos(6\theta_1 + 2\alpha)$$
$$- 4V_\infty r_1^3 a^2 (r_1^4 - a^4) \sin\theta_1 \cos 4\theta_1 + 2V_\infty r_1 a^4 (r_1^4 - a^4) \sin\theta_1 \cos(2\theta_1 - 2\alpha)$$
$$+ 2k_0 r_1^6 (r_1^2 - a^2) \cos(6\theta_1 + 2\alpha) - 4k_0 r_1^4 a^2 (r_1^2 - a^2) \cos 4\theta_1$$
$$+ 2k_0 r_1^2 a^4 (r_1^2 - a^2) \cos(2\theta_1 - 2\alpha) - 2k_1 r_1^6 a^2 \cos(6\theta_1 + 2\alpha)$$
$$- k_1 r_1^4 a^2 (7r_1^2 - 11a^2) \cos 4\theta_1 - 7k_1 r_1^4 a^2 (r_1^2 - a^2) \sin 4\theta_1$$
$$- 2k_1 r_1^2 a^4 (3r_1^2 - 2a^2) \cos(2\theta_1 - 2\alpha) - 6k_1 r_1^2 a^4 (r_1^2 - a^2) \sin(2\theta_1 - 2\alpha)$$
$$- 3(k_1 + m_1)(r_1^2 - a^2)a^6 (\cos 4\alpha - \sin 4\alpha) + 2m_1 r_1^6 a^2 \sin(6\theta_1 + 2\alpha)$$
$$- m_1 r_1^4 a^2 (7r_1^2 - 3a^2) \sin 4\theta_1 - 7m_1 r_1^4 a^2 (r_1^2 - a^2) \cos 4\theta_1$$
$$- 2m_1 r_1^2 a^4 (3r_1^2 - 4a^2) \sin(2\theta_1 - 2\alpha) - 6m_1 r_1^2 a^4 (r_1^2 - a^2) \cos(2\theta_1 - 2\alpha) = 0 \tag{26}$$

3.4 Non-Dimensional Parameters

At this point some non-dimensional parameters have to be introduced if the system of equations (19), (21), (25), and (26) is to be solved explicitly. These are the following:

$$K_0 = \frac{k_0}{aV_\infty} \tag{27}$$

$$K_1 = \frac{k_1}{aV_\infty} \tag{28}$$

$$K = \frac{k}{aV_\infty} \tag{29}$$

$$M_1 = \frac{m_1}{aV_\infty} \tag{30}$$

$$R_1 = \frac{r_1}{a}. \tag{31}$$

Substitution into the original equations yields the following system of four equations in five unknowns K_0, K_1, M_1, R_1, and θ_1:

$$(2\sin\alpha - K)[R_1^2 + 1 - 2R_1\cos(\theta_1 + \alpha)] - 2M_1 R_1 \sin(\theta_1 + \alpha) + K_1(R_1^2 - 1) = 0 \tag{32}$$

$$(2\sin\alpha + K)[R_1^2 + 1 + 2R_1\cos(\theta_1 + \alpha)] - 2M_1 R_1 \sin(\theta_1 + \alpha) - K_1(R_1^2 - 1) = 0 \tag{33}$$

$$
\begin{aligned}
&2R_1^5(R_1^2 - 1)^2 \cos\theta_1 \cos(6\theta_1 + 2\alpha) - 4R_1^3(R_1^2 - 1)^2 \cos\theta_1 \cos 4\theta_1 \\
&\quad + 2R_1(R_1^2 - 1)^2 \cos\theta_1 \cos(2\theta_1 - 2\alpha) - 2R_1^5(R_1^4 - 1)\sin\theta_1 \sin(6\theta_1 + 2\alpha) \\
&\quad + 4R_1^3(R_1^4 - 1)\sin\theta_1 \sin 4\theta_1 - 2R_1(R_1^4 - 1)\sin\theta_1 \sin(2\theta_1 - 2\alpha) \\
&\quad - 2K_0 R_1^6(R_1^2 - 1)\sin(6\theta_1 + 2\alpha) + 4K_0 R_1^4(R_1^2 - 1)\sin 4\theta_1 \\
&\quad - 2K_0 R_1^2(R_1^2 - 1)\sin(2\theta_1 - 2\alpha) + 2K_1 R_1^6 \sin(6\theta_1 + 2\alpha) \\
&\quad + K_1 R_1^4(7R_1^2 - 11)\sin 4\theta_1 + 7K_1 R_1^4(R_1^2 - 1)\cos 4\theta_1 \\
&\quad + 2K_1 R_1^2(3R_1^2 - 2)\sin(2\theta_1 - 2\alpha) + 6K_1 R_1^2(R_1^2 - 1)\cos(2\theta_1 - 2\alpha) \\
&\quad + 3(K_1 - M_1)(R_1^2 - 1)(\cos 4\alpha - \sin 4\alpha) + 2M_1 R_1^6 \cos(6\theta_1 + 2\alpha) \\
&\quad - M_1 R_1^4(7R_1^2 - 3)\cos 4\theta_1 - 7M_1 R_1^4(R_1^2 - 1)\sin 4\theta_1 \\
&\quad - 2M_1 R_1^2(3R_1^2 - 4)\cos(2\theta_1 - 2\alpha) - 6M_1 R_1^2(R_1^2 - 1)\sin(2\theta_1 - 2\alpha) = 0 \tag{34}
\end{aligned}
$$

$$
\begin{aligned}
&2R_1^5(R_1^2 - 1)^2 \cos\theta_1 \sin(6\theta_1 + 2\alpha) - 4R_1^3(R_1^2 - 1)^2 \cos\theta_1 \sin 4\theta_1 \\
&\quad + 2R_1(R_1^2 - 1)^2 \cos\theta_1 \sin(2\theta_1 - 2\alpha) + 2R_1^5(R_1^4 - 1)\sin\theta_1 \cos(6\theta_1 + 2\alpha)
\end{aligned}
$$

$$-4R_1^3(R_1^4 - 1)\sin\theta_1\cos 4\theta_1 + 2R_1(R_1^4 - 1)\sin\theta_1\cos(2\theta_1 - 2\alpha)$$

$$+2K_0 R_1^6(R_1^2 - 1)\cos(6\theta_1 + 2\alpha) - 4K_0 R_1^4(R_1^2 - 1)\cos 4\theta_1$$

$$+2K_0 R_1^2(R_1^2 - 1)\cos(2\theta_1 - 2\alpha) - 2K_1 R_1^6\cos(6\theta_1 + 2\alpha)$$

$$-K_1 R_1^4(7R_1^2 - 11)\cos 4\theta_1 - 7K_1 R_1^4(R_1^2 - 1)\sin 4\theta_1$$

$$-2K_1 R_1^2(3R_1^2 - 2)\cos(2\theta_1 - 2\alpha) - 6K_1 R_1^2(R_1^2 - 1)\sin(2\theta_1 - 2\alpha)$$

$$-3(K_1 + M_1)(R_1^2 - 1)(\cos 4\alpha - \sin 4\alpha) + 2M_1 R_1^6\sin(6\theta_1 + 2\alpha)$$

$$-M_1 R_1^4(7R_1^2 - 3)\sin 4\theta_1 - 7M_1 R_1^4(R_1^2 - 1)\cos 4\theta_1$$

$$-2M_1 R_1^2(3R_1^2 - 4)\sin(2\theta_1 - 2\alpha) - 6M_1 R_1^2(R_1^2 - 1)\cos(2\theta_1 - 2\alpha) = 0 \qquad (35)$$

3.5 Additional Condition

We see that the equations derived so far are not enough to give us a unique solution. Therefore we must seek additional information in the nature of the flow. As mentioned in the introduction the flow is assumed inviscid which implies that the total force on the plate must be perpendicular to it (see Figure 4). Therefore

$$\tan\alpha = \frac{D}{L} \qquad (36)$$

Now we have to relate the drag and the lift with the unknowns K and M_1.

From Figure 5 we see that the fluid between streamlines a and b disappears into the sink producing drag which can be calculated as follows: The rate of mass of fluid between the streamlines a and b (which is distance d apart) must be equal to the rate with which mass is disappearing in the sink, i.e.,

$$\dot{m} = -\rho V_\infty db = m_1\rho b 2\pi. \qquad (37)$$

Now the drag is given by the rate of loss of momentum of that fluid therefore

$$D = -\dot{m}V_\infty \qquad (38)$$

combining equations (37) and (38) we get

$$m_1 = -\frac{D}{2\pi\rho b V_\infty} \qquad (39)$$

and from equation (30) we get

$$M_1 = -\frac{D}{2\pi\rho b a V_\infty^2} \qquad (40)$$

but

$$S = bc \qquad (41)$$

and from the Joukowski transformation we know that

$$c = 4a \qquad (42)$$

also,

$$C_D = \frac{D}{\frac{1}{2}\rho V_\infty^2 S}. \qquad (43)$$

The last four equations combine to give

$$C_D = -\pi M_1 \qquad (44)$$

The lift can be found from the Kutta-Joukowski law

$$L = \rho V_\infty \Gamma \cdot b \qquad (45)$$

and since

$$\Gamma = 2\pi k \qquad (46)$$

and

$$C_L = \frac{L}{\frac{1}{2}\rho V_\infty^2 S} \qquad (47)$$

we get

$$C_L = \pi K \qquad (48)$$

after employing equation (29).

Now going back to equation (36) we see that

$$\tan\alpha = -\frac{M_1}{K} \qquad (49)$$

thus we have a system of five equations (32)–(35) and (49), which can be solved for the five unknowns: R_1, θ_1, K_0, K_1, and M_1. This is done numerically (see Appendix 2) and the results are shown in the next section.

4. RESULTS

4.1 Position of the Equilibrium Point

As it can be seen from Figure 6 the equilibrium point is always ahead of the leading edge of the plate and it goes farther as the angle of attack increases reaching a maximum distance of approximately 53 percent of the chord from the leading edge (measured along the chord line) at 45 degrees angle of attack.

At the same time (see Figure 7) after reaching a maximum distance above the chord line of approximately 16 percent of the chord (measured perpendicular to the chord line), it starts moving downwards crossing the chord line at $\alpha \simeq 35°$ and getting farther under it at higher angles of attack.

4.2 Vortex and Sink Strengths

The bound vortex strength increases almost linearly with angle of attack while the leading edge vortex strength grows nonlinearly reaching a maximum at $\alpha = 45°$ and dropping to zero at $\alpha \simeq 73°$ where the lower stagnation point reaches the trailing edge and moves off the plate (Figure 8). Thus the total circulation is also nonlinear with angle of attack and has a maximum at $\alpha = 50°$ (Figure 10). The sink strength on the other hand, starting with very small values increases almost linearly with angle of attack (Figure 9).

4.3 Pressure Distribution on the Plate

The pressure distribution has been calculated at the ς' plane (the most convenient one since the plate is horizontal and lies along the ξ'-axis).

From the sequence of transformations shown in Figure 2 we have

$$\varsigma' = z' + \frac{a^2}{z'}$$

$$= ze^{i\alpha} + \frac{a^2}{z}e^{-i\alpha}$$

$$= re^{i\theta}e^{i\alpha} + \frac{a^2}{r}e^{-i\alpha}e^{-i\theta}$$

or

$$\varsigma' = r\left[\cos(\theta + \alpha) + i\sin(\theta + \alpha)\right] + \frac{a^2}{r}\left[\cos(\theta + \alpha) - i\sin(\theta + \alpha)\right].$$

and since

$$\varsigma' = \xi' + i\eta' \tag{50}$$

we have

$$\xi' = \left(r + \frac{a^2}{r}\right)\cos(\theta + \alpha) \tag{51}$$

and

$$\eta' = \left(r - \frac{a^2}{r}\right)\sin(\theta + \alpha) \tag{52}$$

on the surface of the plate $r = a$ so

$$\xi'_{sp} = 2a\cos(\theta + \alpha) \tag{53}$$

$$\eta'_{sp} = 0 \tag{54}$$

To find the velocity field around the plate, a similar procedure as in Section 2.3 yields:

$$\frac{dw}{d\varsigma'} = \frac{dw}{dz} \cdot \frac{dz}{d\varsigma'}$$

$$= \frac{dw}{dz} \cdot \frac{z^2}{z^2 e^{i\alpha} - a^2 e^{-i\alpha}}$$

or

$$e^{-i\theta}(u_{r_p} - iu_{\theta_p}) = e^{-i\theta}(u_{r_s} - iu_{\theta_s}) \cdot \frac{r^2 e^{i2\theta}}{r^2 e^{i(2\theta+\alpha)} - a^2 e^{-i\alpha}}$$

and on the surface $(r = a)$ we get finally

$$u_{r_{sp}} = -\frac{1}{2} \cdot \frac{\cos\theta}{\sin(\theta + \alpha)} u_{\theta_{ss}} \tag{55}$$

$$u_{\theta_{sp}} = -\frac{1}{2} \cdot \frac{\sin\theta}{\sin(\theta + \alpha)} u_{\theta_{ss}} \tag{56}$$

from which

$$u_{sp} = \frac{1}{2} u_{\theta_{ss}} \csc(\theta + \alpha) \tag{57}$$

Now from equation (5) and using equations (27)-(31) we find that

$$\frac{u_{\theta_{ss}}}{V_\infty} = -2\sin\theta - K + \frac{2M_1 R_1 \sin(\theta - \theta_1) + K_1(R_1^2 - 1)}{1 + R_1^2 - 2R_1 \cos(\theta - \theta_1)} \tag{58}$$

48

Substituting equation (58) into (57) as well as the corresponding solution sets for each angle of attack we can find the pressure distribution from

$$C_{p_{sp}} = 1 - \frac{u_{sp}^2}{V_\infty^2} \tag{59}$$

$C_{p_{sp}}$ has been plotted for four angles of attack in Figure 11 where the horizontal axis measures the non-dimensional parameter

$$n = \cos(\theta + \alpha) = \frac{\xi'_{sp}}{2a}$$

which varies from -1 at the leading edge to $+1$ at the trailing edge.

It can be seen from the plottings that both stagnation points move towards the trailing edge as the angle of attack increases but the lower one moves faster, being at about 70 percent of the chord from the leading edge at $\alpha = 60°$ while the upper one is only at the mid-chord point.

4.4 Lift, Drag, and Pitching Moment

At this point a comparison will be made between the results of:

(i) the classical solution of totally attached flow over the plate with the Kutta condition satisfied at the trailing edge only and a singularity (infinite suction) at the leading edge (Figure 12a),

(ii) this model with a detached vortex and a sink which make possible the satisfaction of the Kutta condition at both edges removing thus the leading edge singularity (Figure 12b),

(iii) the Helmholtz solution of totally separated flow over the plate (Figure 12c).

The lift, drag and moment coefficients for the three models are given below:

$$C_{L1} = 2\pi \sin \alpha \qquad C_{D1} = 0 \qquad C_{M1} = \frac{\pi}{4} \sin 2\alpha \tag{60}$$

$$C_{L2} = \pi K \qquad C_{D2} = -\pi M_1 \qquad C_{M2} = \frac{\pi}{4} \sin 2\alpha \tag{61}$$

$$C_{L3} = \frac{\pi \sin 2\alpha}{4 + \pi \sin \alpha} \qquad C_{D3} = \frac{2\pi \sin^2 \alpha}{4 + \pi \sin \alpha} \tag{62}$$

From Figure 13 it can be seen that our model with partially separated flow (as the leading edge vortex can be thoug't of), gives the h'ghest lift coefficient at least up to $\alpha = 60°$.

At higher angles it looks like the first model gives slightly higher lift coefficients, but this is misleading since at high angles of attack the flow separates at some point on the upper surface, resulting in significantly lower lift coefficients. Thus the first model breaks down at high angles of attack.

From Figure 14 it can be seen that our model gives much higher drag coefficients even than the third model in which the flow is totally separated on the upper surface of the plate. This should not be surprising however, because the drag in our model is associated with a large momentum loss of all the fluid that dissappears into the sink (see Figure 5).

As a confirmation to the above comes Figure 15 which shows the same lift to drag ratio for the second and third models (since $L/D = \tan \alpha$ in both cases). In other words since the second model yields a much higher lift than the third one, it also gives a much higher drag which can be thought of as induced drag (lift related drag).

Finally, it is interesting to note that our model has the same moment coefficient and the same position of aerodynamic center (at the quarter chord point) as the first model. The proof is as follows: Since there is a uniform wind, the velocity at a great distance from the plate must tend simply to the wind velocity, and therefore if $|z|$ is sufficiently large we may write

$$\frac{dw}{dz} = V_\infty + \frac{A}{z} + \frac{B}{z^2} + \cdots$$

or

$$w = V_\infty z + A \ln z + \frac{B}{z} + \cdots.$$

Now the force and the moment on the plate can be found from the theorem of Blasius and it turns out (after performing the integration) that the force depends only on A while the moment depends only on B. However, comparing the complex potential for the first two models we can see that B is the same regardless of the presence of the vortex/sink combination and therefore the moment ought to be the same for the two models. In equations (60) and (61) C_M is taken about the mid-point of the plate and is therefore positive. The same relations but with a minus sign on the right hand side are valid for C_M about the leading edge. Equations (60) and (61) are plotted in Figure 16.

5. CONCLUSIONS

(i) The present inviscid, incompressible, two-dimensional model of a flat plate with a detached vortex close to its leading edge indicates that lift coefficients up to around 6 are achievable. Higher values should also be possible if thickness and camber are added, considering an airfoil instead of a flat plate (reference 3).

(ii) In order to satisfy the Kutta condition at both the trailing edge and the leading edge, the presence of the sink is necessary (see equations (32) and (33)). This is in agreement with physical observations of the leading edge vortex which forms over delta wings at high angles of attack where the spanwise pressure gradient due to sweep angle evacuates the vortex core. It is also in agreement with the model presented in reference 3.

(iii) For a given lift (C_L) there are two possible solutions for the location of the equilibrium point and the corresponding strengths of the vortex and sink. That of the lower angle of attack gives a weaker sink and therefore less drag, while that of the higher angle of attack gives a stronger sink and the associated higher drag. The vortex strengths do not differ much for the two solutions since they are closely related to the lift (which is the same for the two solutions). This result is also in agreement with reference 3.

(iv) The upper limit found in the C_L versus α curve suggests that if a stronger vortex would exist at the equilibrium point, unrealistic supercirculation would occur resulting in the streamlines going entirely around the system.

(v) A limitation of the present model appears at $\alpha \simeq 73°$, above which the lower stagnation point moves off the plate making thus impossible the flow pattern depicted in Figure 5, on which this model is based.

(vi) A comparison between Figures 8 and 1c shows very good agreement (at least qualitatively) between the results derived here and those found experimentally in reference 1.

(vii) Finally, the presence of the vortex and the sink does not affect the position of the aerodynamic center which remains at the quarter chord point.

REFERENCES

1. Hummel, D. "On the Vortex Formation Over a Slender Wing at Large Angles of Incidence," *AGARD CP-247, no. 15*, 1978.

2. Milne-Thomson, L. M. *Theoretical Aerodynamics*. New York: Dover, 1958.

3. Rossow, V. J. "Lift Enhancement by an Externally Trapped Vortex," *J. Aircraft, 15, no. 9* (1978), 618.

4. Milne-Thomson, L. M. *Theoretical Hydrodynamics*, London: MacMillan Press, 1968.

5. Rossow, V. J. "On the Inviscid Rolled-Up Structure of Lift-Generated Vortices," *J. Aircraft, 10, no. 11* (1973), 647.

6. Hoeijmakers, H.W.M. and B. Bennekers, "A Computational Model for the Calculation of the Flow About Wings With Leading-Edge Vortices," *AGARD CP-247, no. 25*, 1978.

7. Bradley, R. G., C. W. Smith, and I. C. Bhateley, "Vortex-Lift Prediction for Complex Wing Planforms," *J. Aircraft, 10, no. 6* (1973), 379.

8. Peake, D. J. and M. Tobak, "Three-Dimensional Flows About Simple Components at Angle of Attack," *AGARD LS-121, no. 2*, 1982.

9. Skow, A. M. and G. E. Erickson, "Modern Fighter Aircraft Design for High Angle of Attack Maneuvering," *AGARD LS-121, no. 4*, 1982.

10. Lamar, J. E. and J. F. Campbell, "Recent Studies at NASA-Langley of Vortical Flows Interacting With Neighbouring Surfaces," *AGARD CP-342, no. 10*, 1983.

Figures

(a)

a. Vortex formation.

(b)

b. Pressure distribution

(c)

c. Lift characteristic.
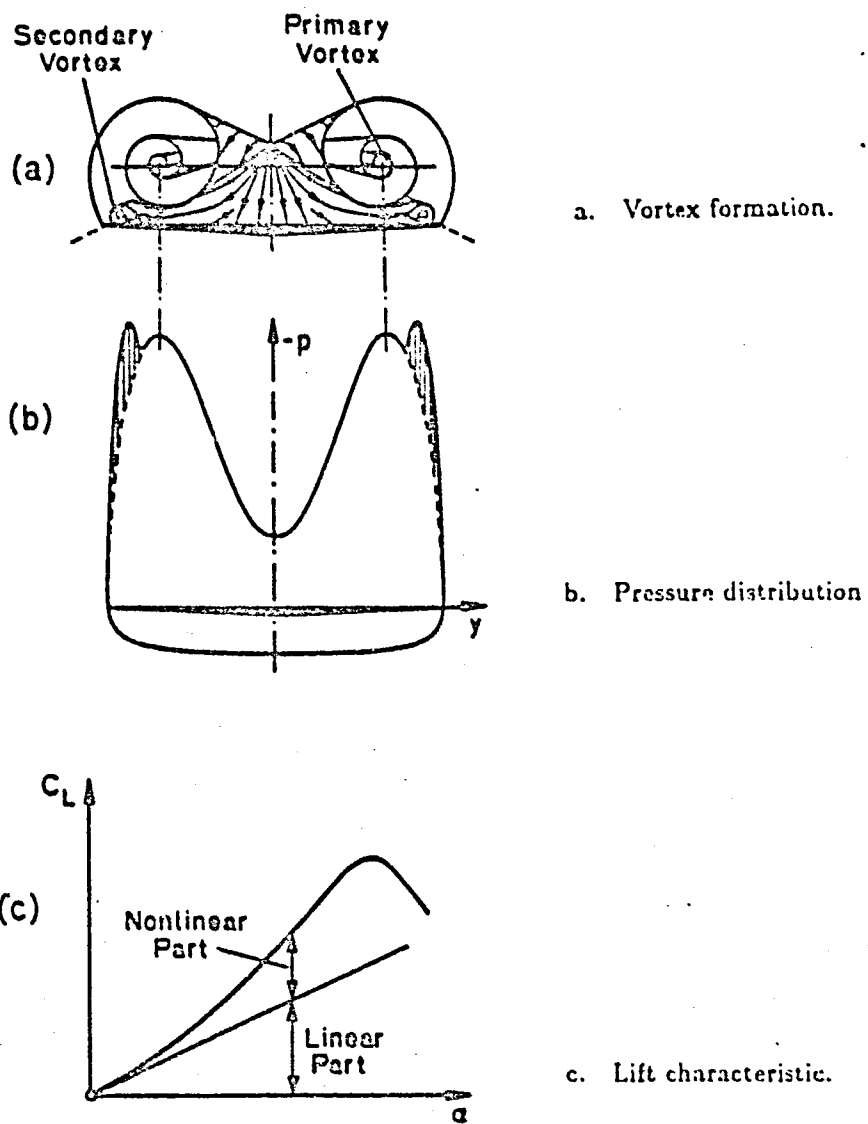
Figure 1. Schematic of the flow over a slender sharp-edged wing.
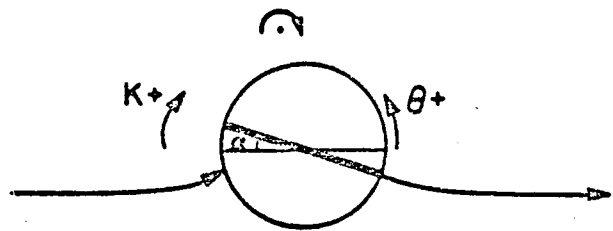
a. Original circle plane (z-plane).
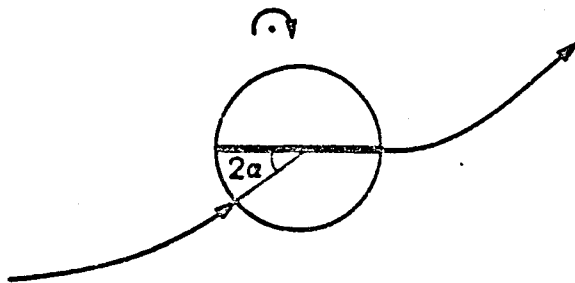
b. Rotated circle plane (z'-plane).
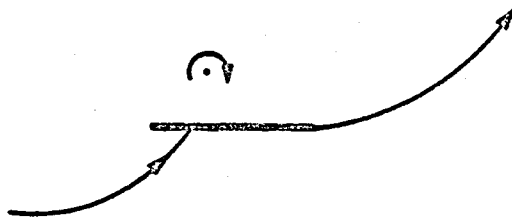
c. Joukowski plane (ς'-plane).

d. Final plate plane (ς-plane).

Figure 2. Steps in mapping sequence from original circle plane to final flat airfoil plane.
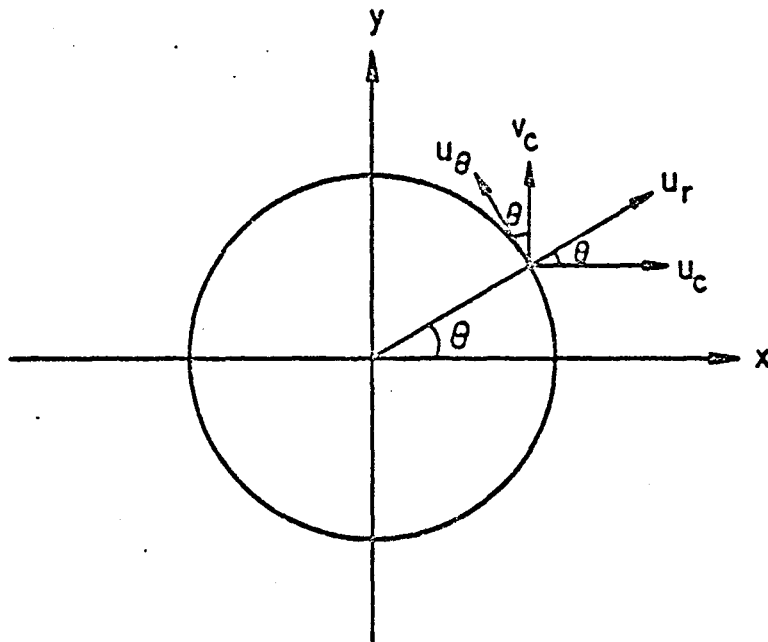
Figure 3. Velocity components in cartesian and polar coordinate systems.
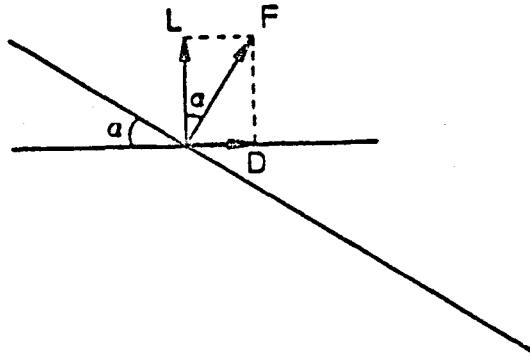
Figure 4. Force diagram on the flat plate.
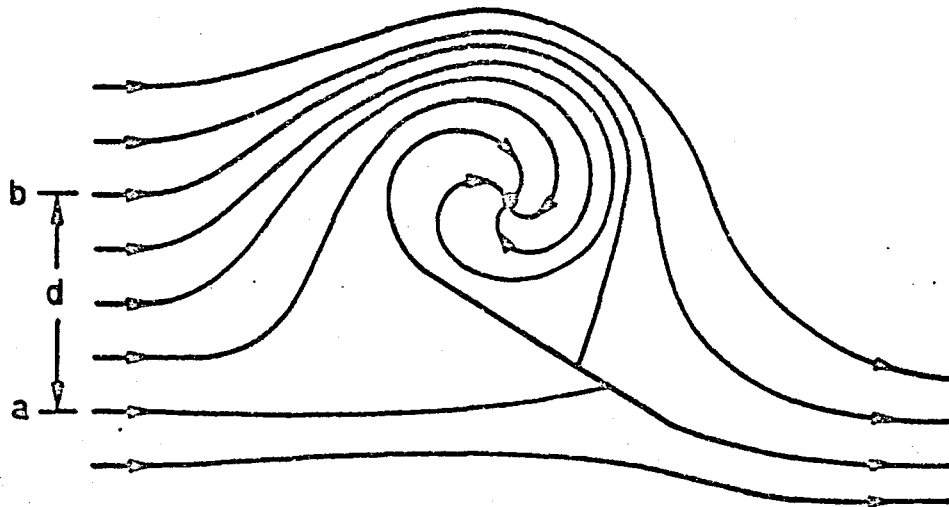
Figure 5. Streamline pattern around the flat plate at an angle of attack with a detached vortex and a sink.
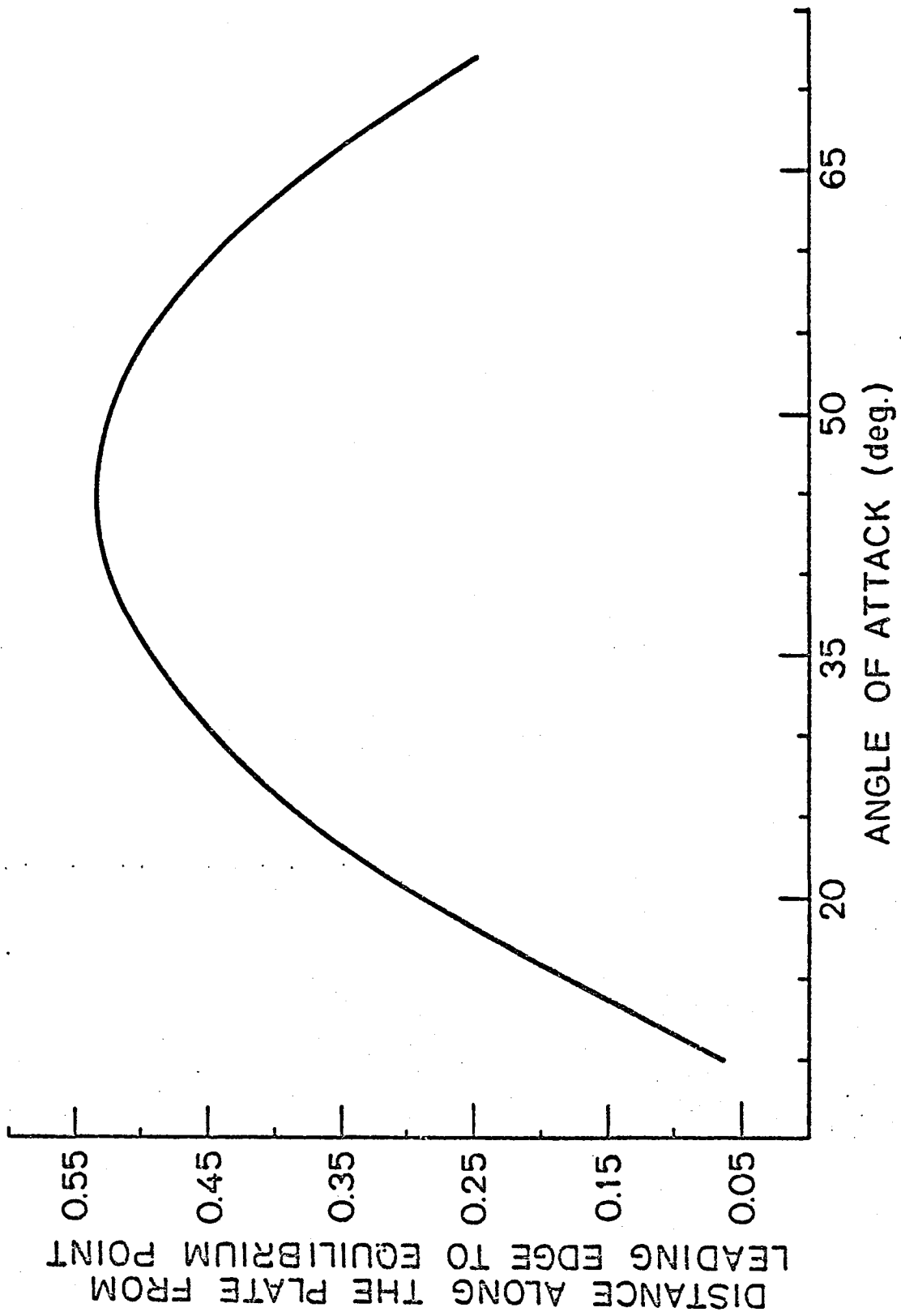
Figure 6.   Position of the equilibrium point (along the plate).

DISTANCE ALONG THE PLATE FROM LEADING EDGE TO EQUILIBRIUM POINT

ANGLE OF ATTACK (deg.)

58
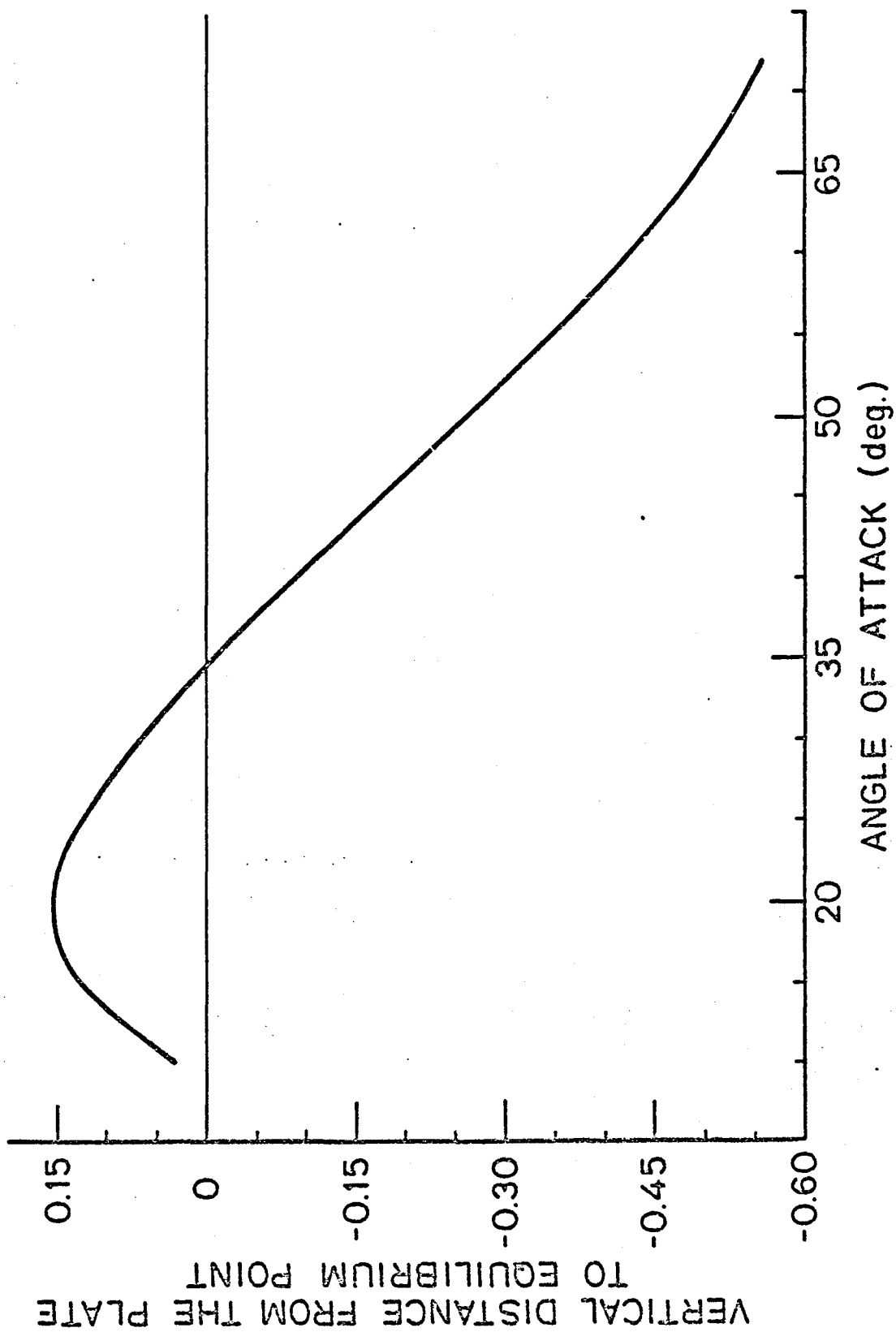
Figure 7.   Position of the equilibrium point (perpendicular to the plate).
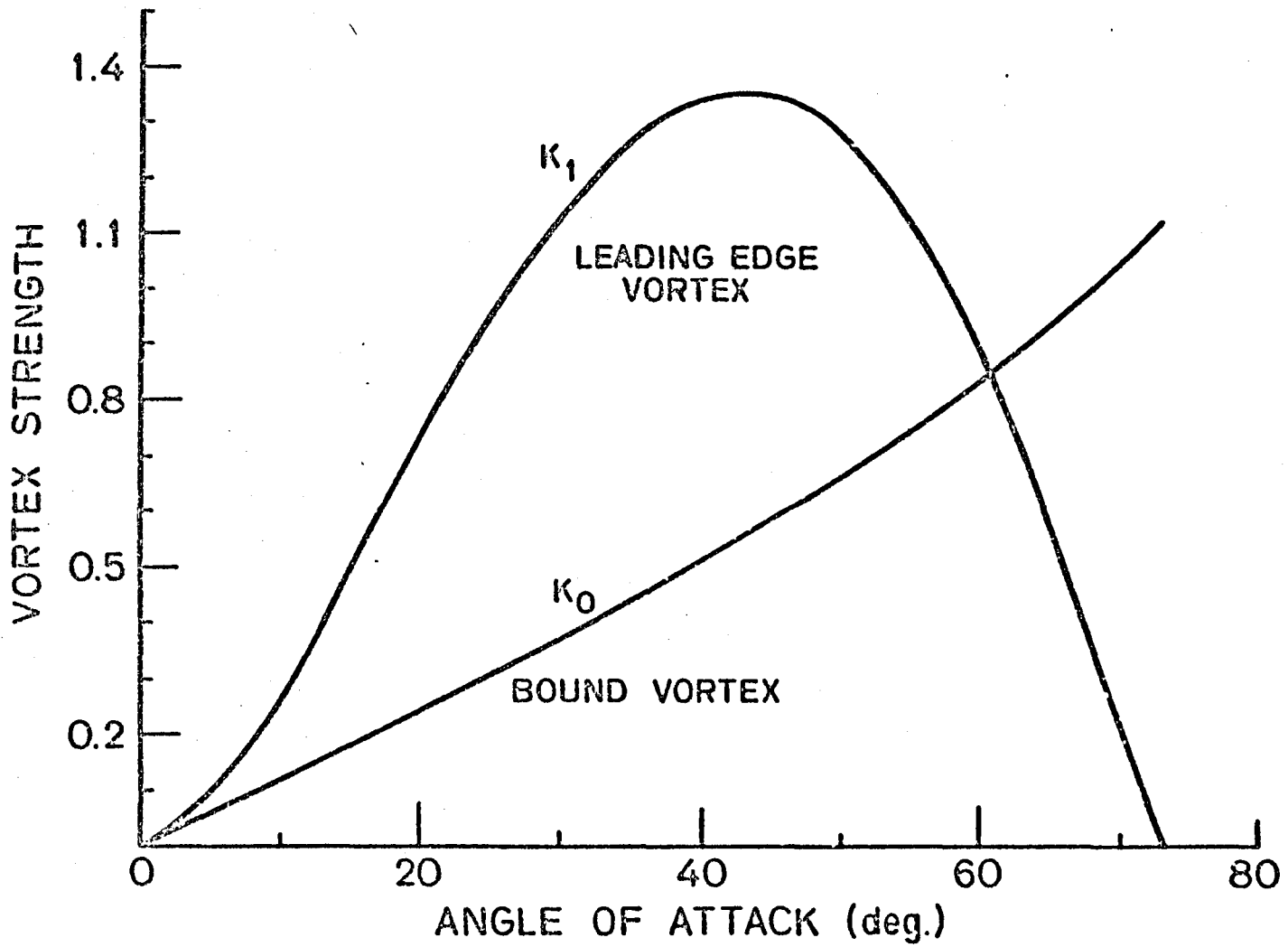
Figure 8. Leading edge and bound vortex strength versus angle of attack.
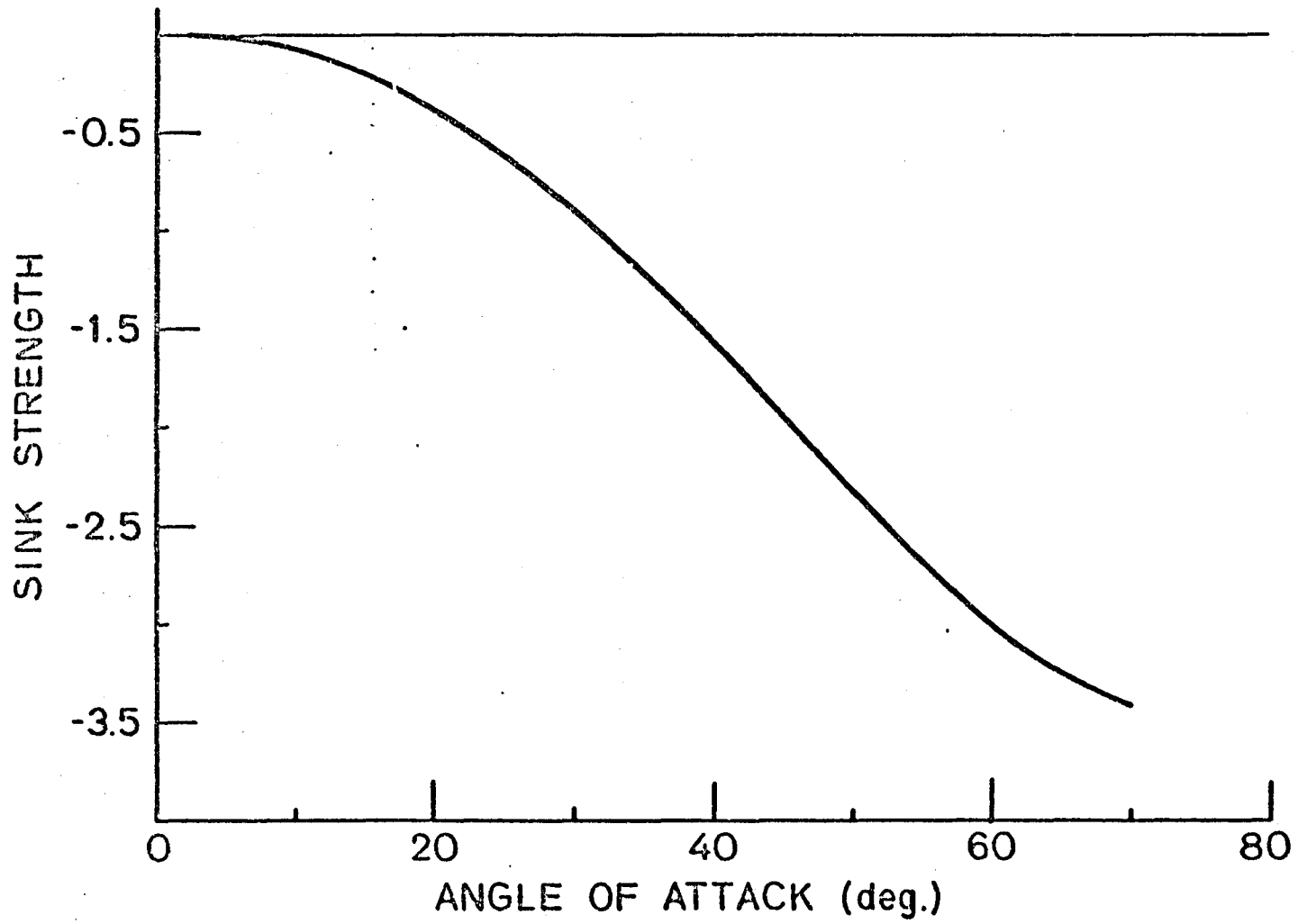
Figure 9. Sink strength versus angle of attack.
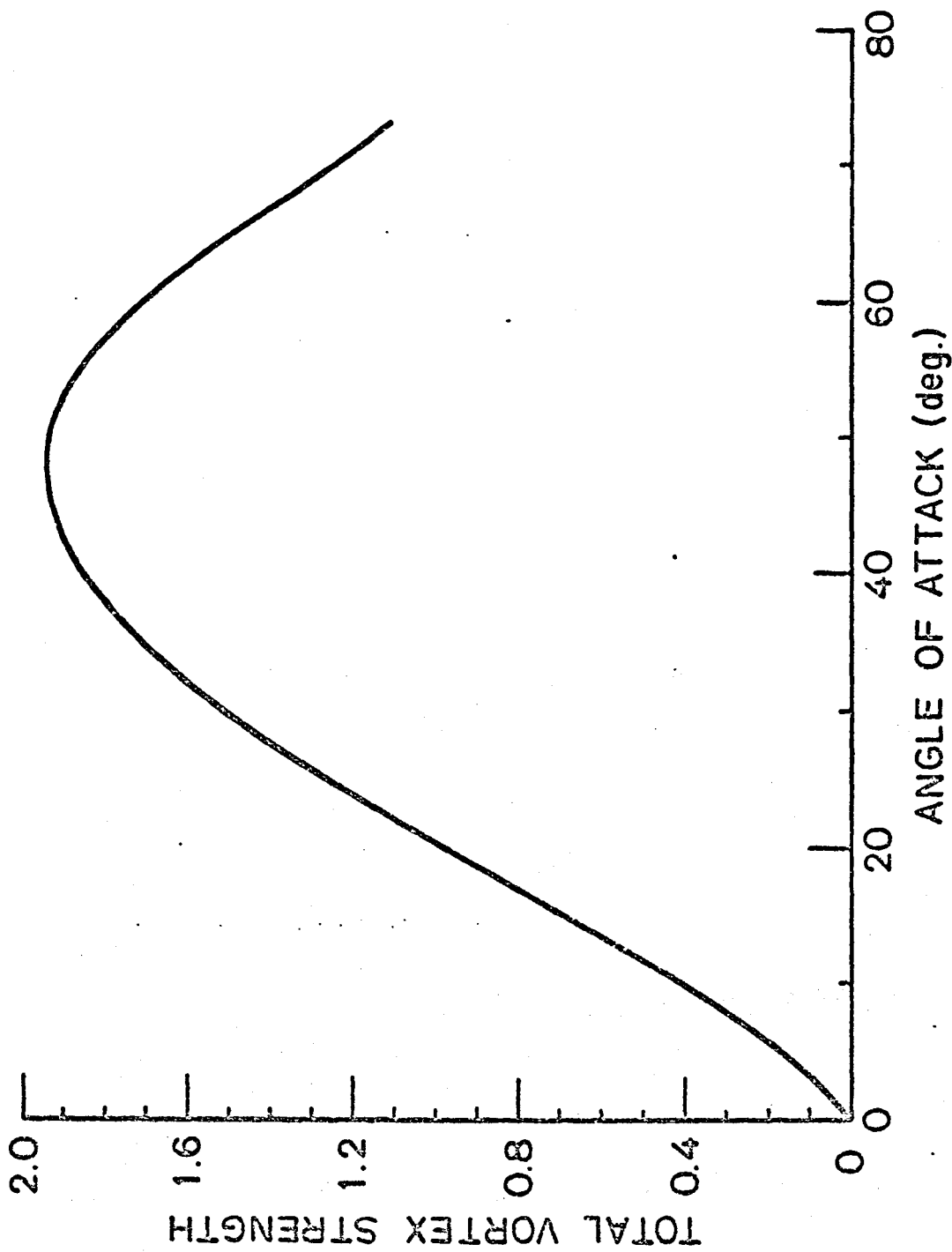
Figure 10. Total vortex strength versus angle of attack.
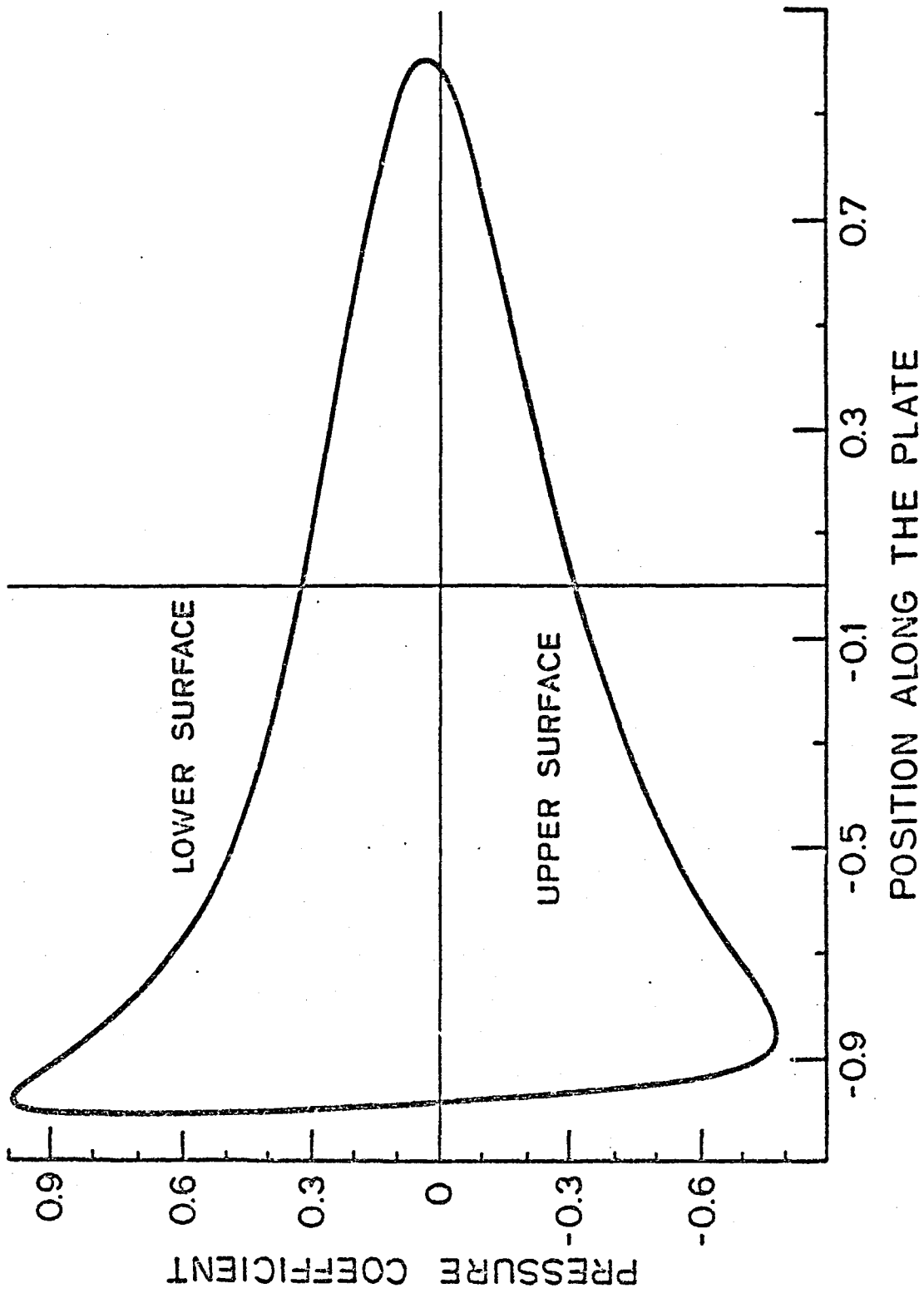
Figure 11a. Pressure distribution along the plate for $\alpha = 10$ deg.
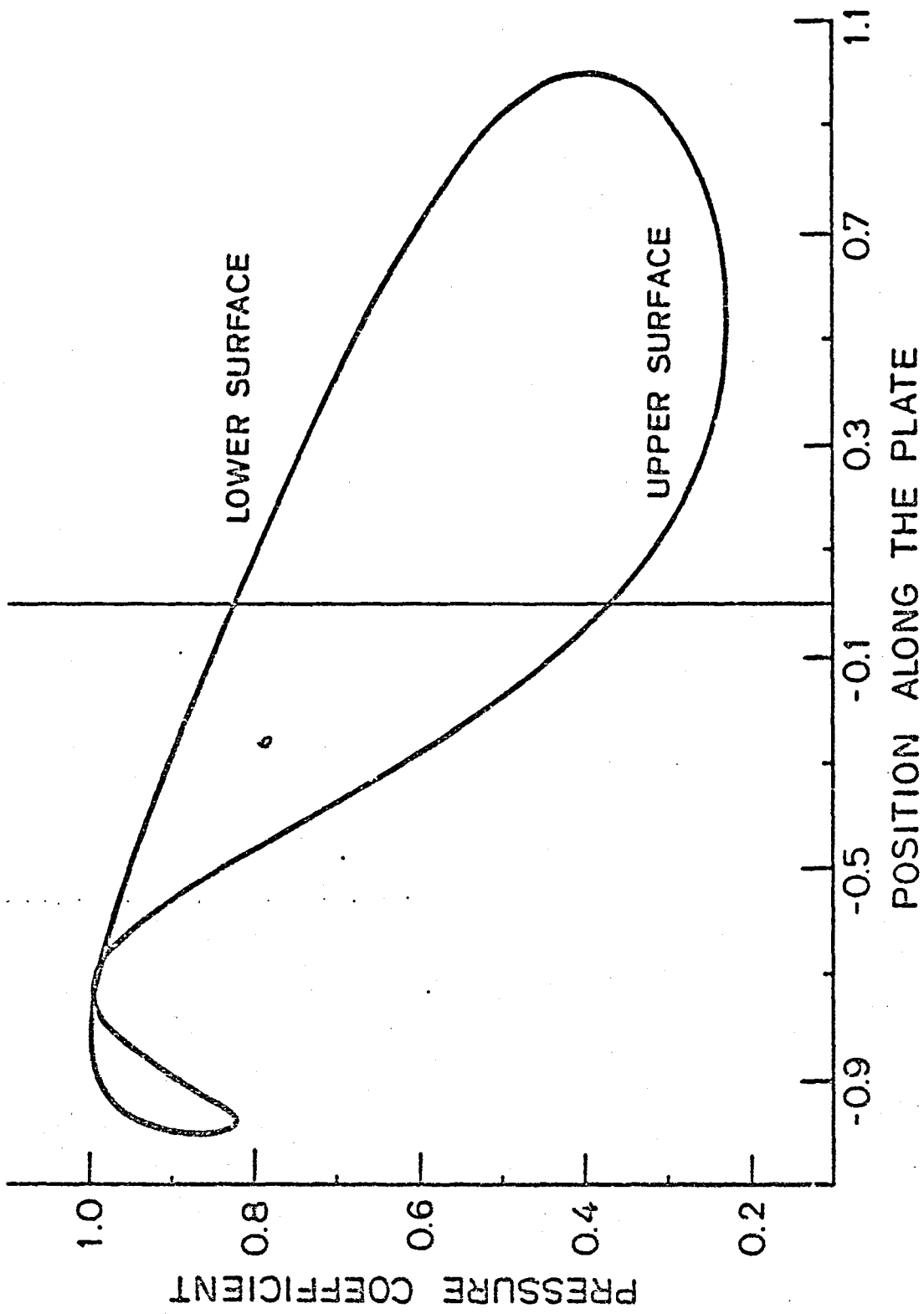
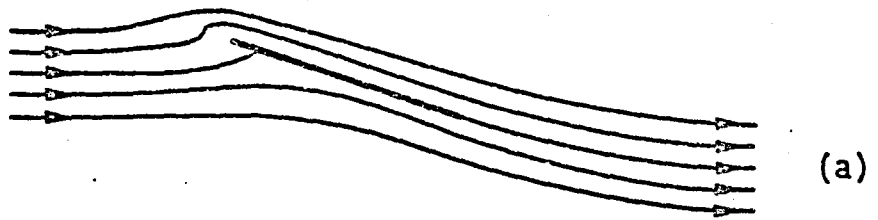Figure 11b. Pressure distribution along the plate for α = 30 deg.
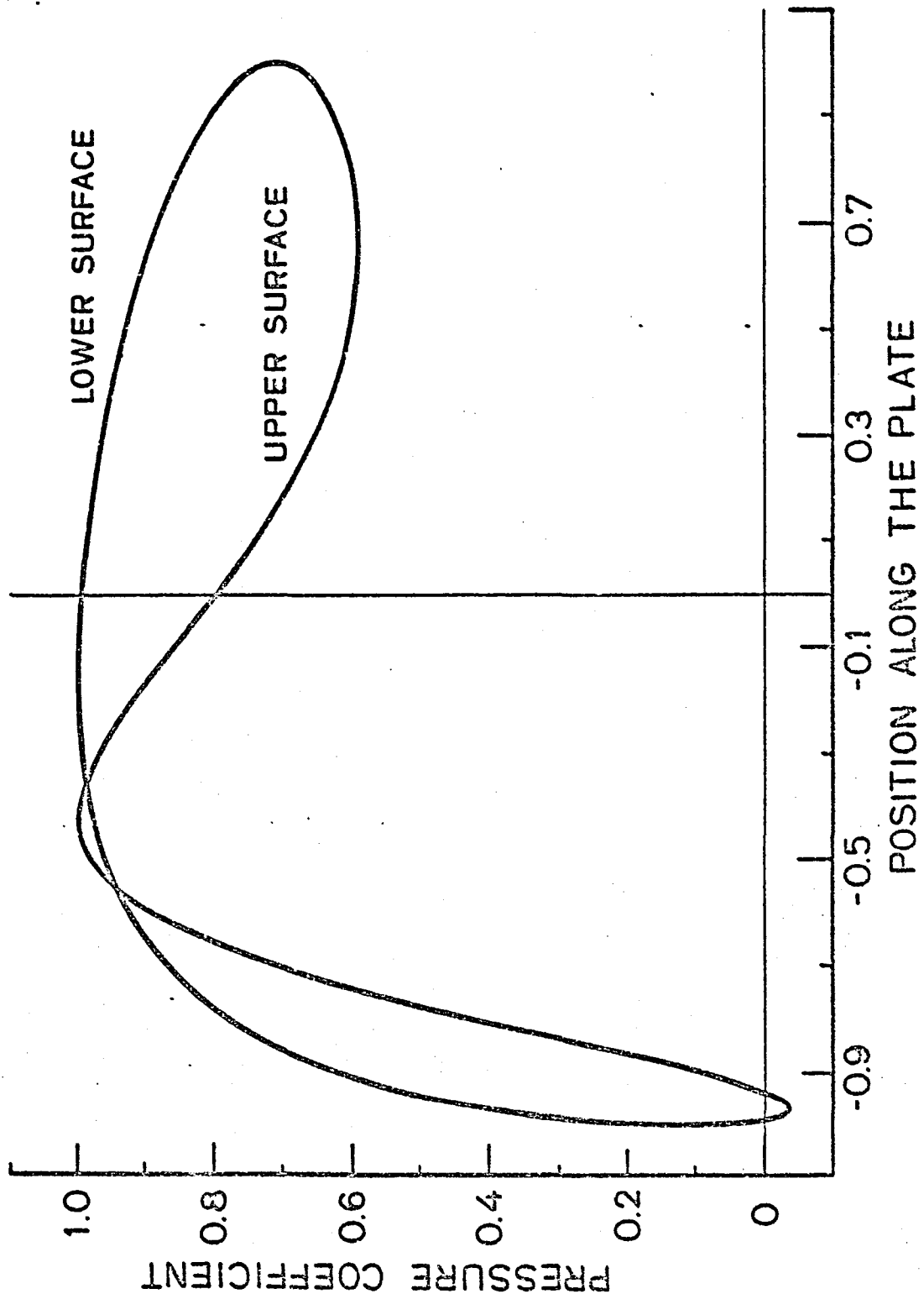
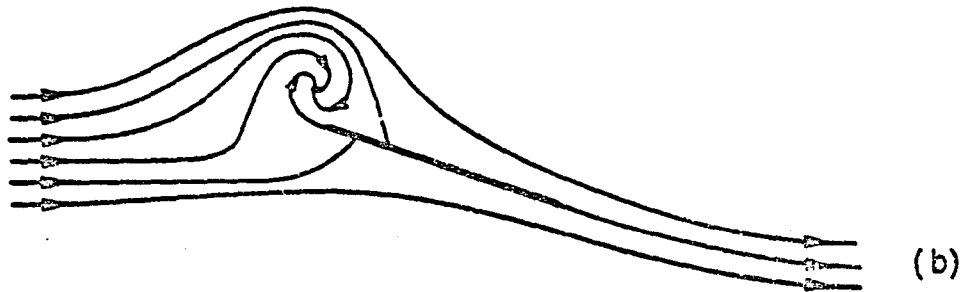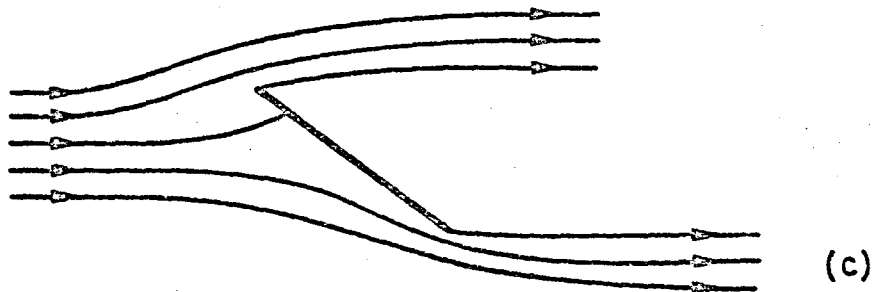Figure 11c. Pressure distribution along the plate for $\alpha = 45$ deg.
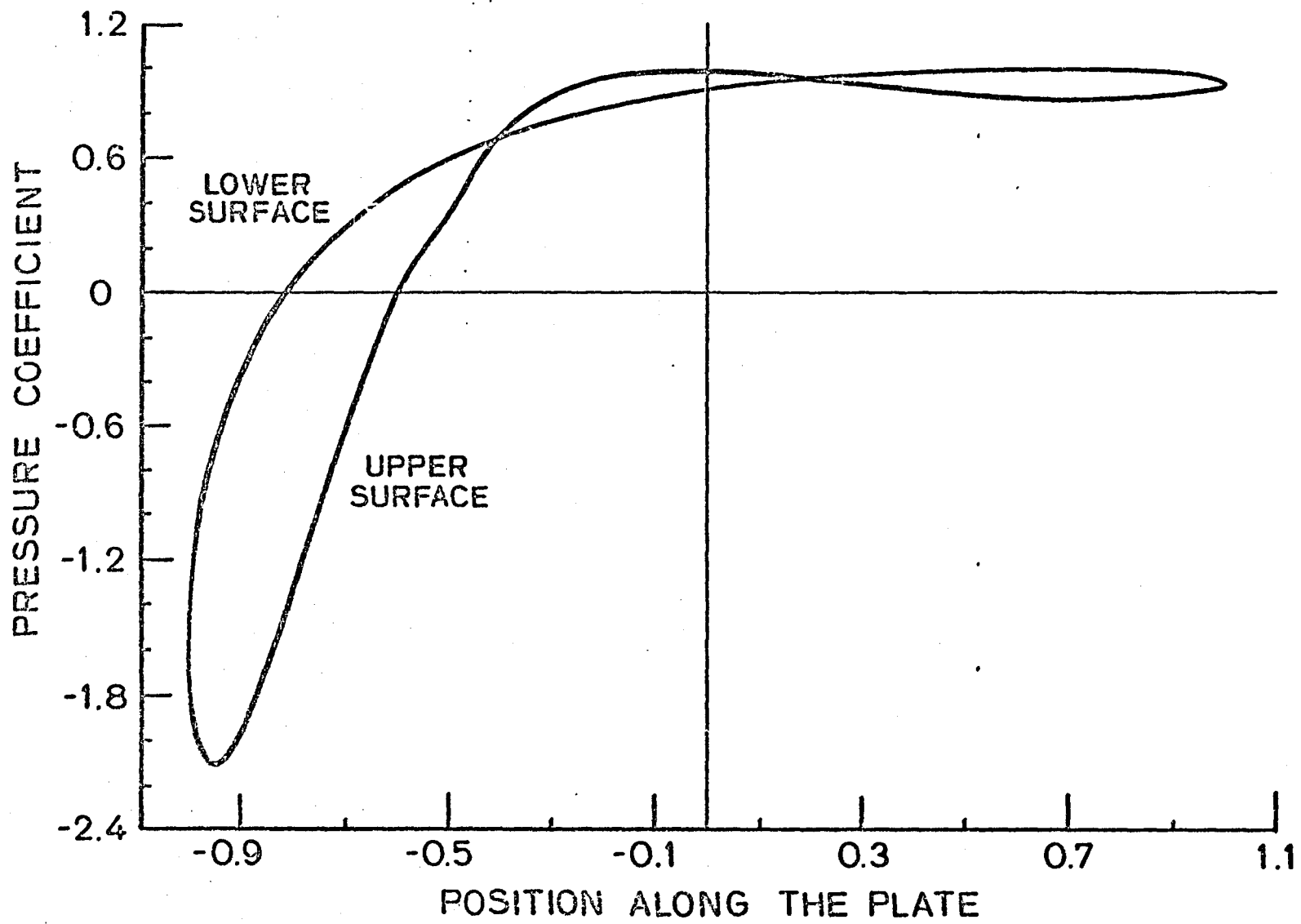
Figure 11d. Pressure distribution along the plate for $\alpha = 60$ deg.

a. Totally attached flow.

b. Partially separated flow.

c. Totally separated flow.

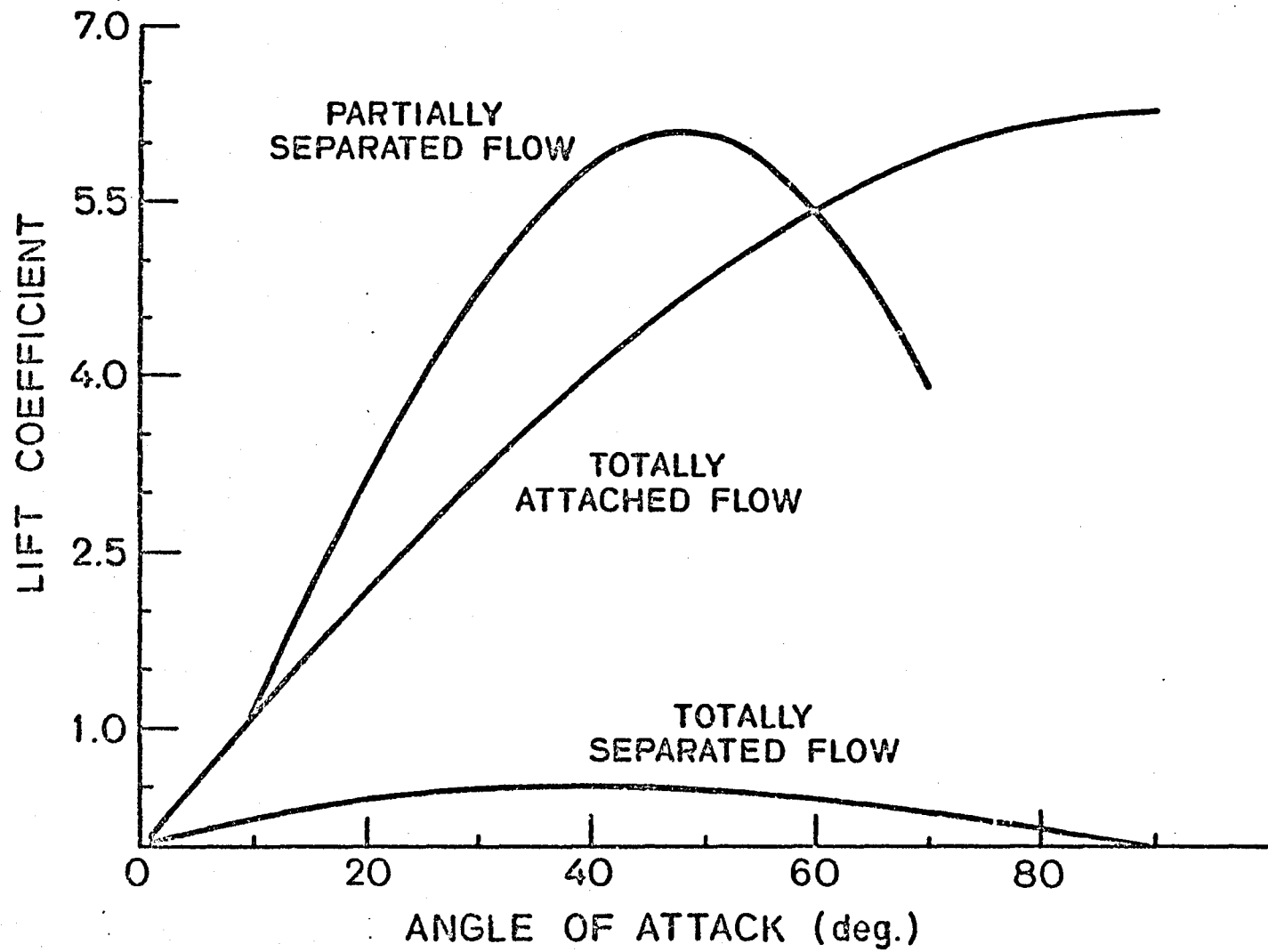*Figure 12.* Schematic of the flow over a flat plate at an angle of attack, according to three different models.

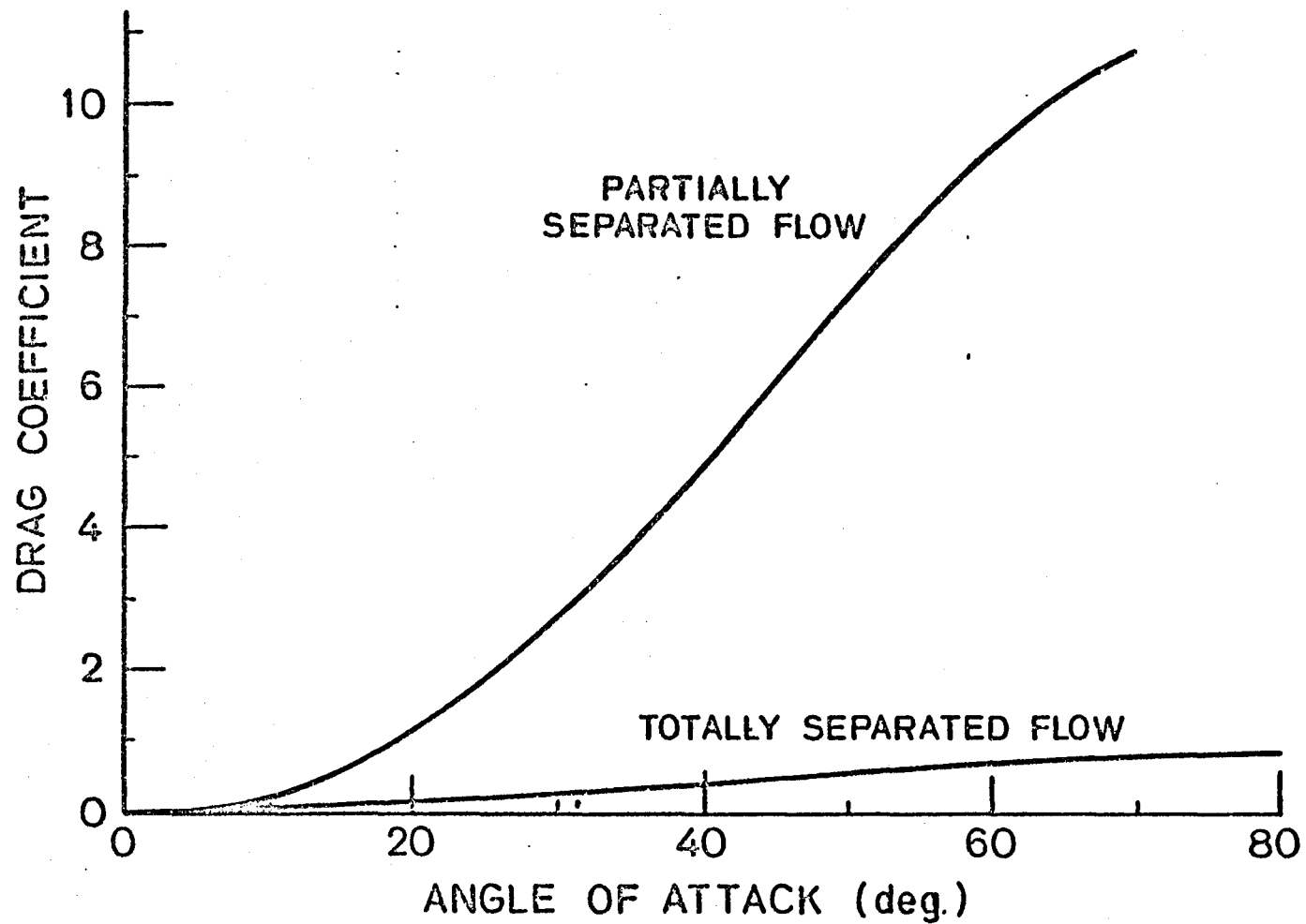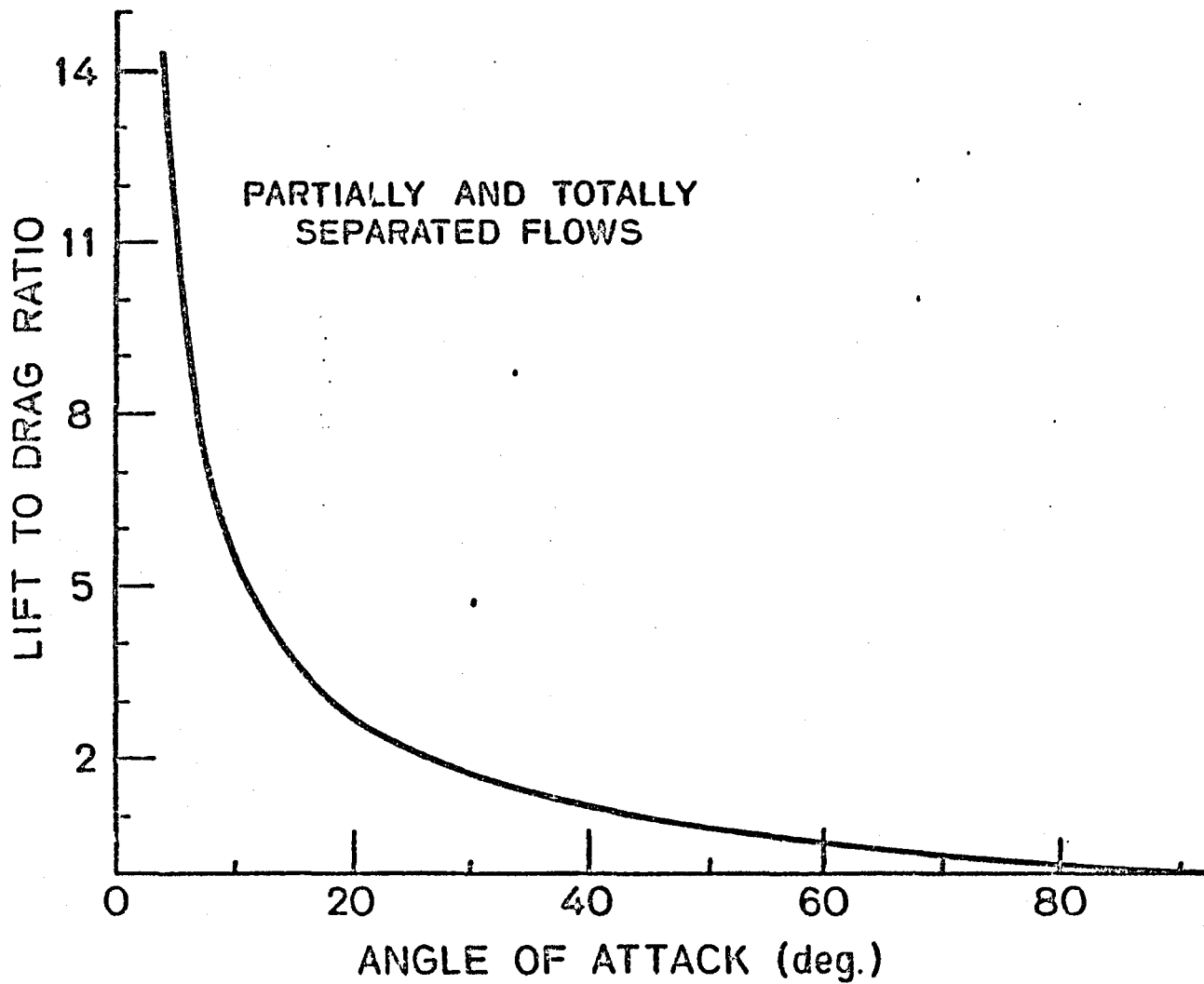Figure 13. , Lift characteristics.

Figure 14. Drag characteristics.

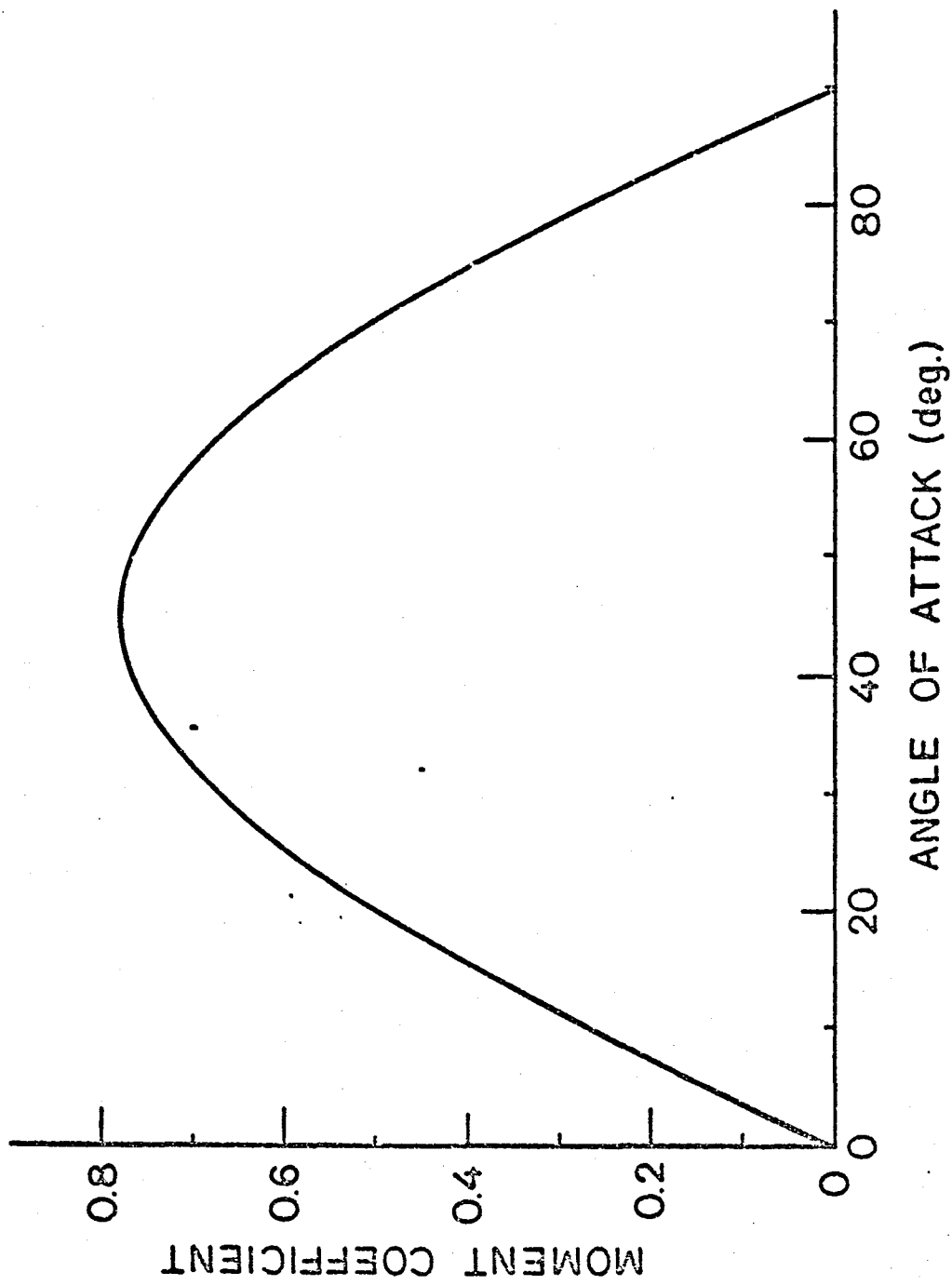Figure 15.   Lift to drag ratio versus angle of attack.

Figure 16. Pitching moment characteristic.

APPENDIX 1

A1.1

Consider a vortex of strength k_1 at the point z_1 outside of a cylinder $|z| = a$. Then, the complex potential is

$$w = f(z) + \bar{f}\left(\frac{a^2}{z}\right)$$

$$= ik_1 \ln(z - z_1) - ik_1 \ln\left(\frac{a^2}{z} - \bar{z}_1\right)$$

according to the circle theorem (reference 2) w can also be written as

$$w = ik_1 \ln z + ik_1 \ln(z - z_1) - ik_1 \ln\left(z - \frac{a^2}{\bar{z}_1}\right) + \text{const.}$$

which shows three vortices: one at the point z_1; one at the point $\frac{a^2}{\bar{z}_1}$ which is the inverse square point of z_1 with respect to the cylinder; and one at the origin (center of the cylinder).

A1.2

Consider a sink of strength m_1 at the point z_1 outside of a cylinder $|z| = a$. Then, the complex potential is

$$w = f(z) + \bar{f}\left(\frac{a^2}{z}\right)$$

$$w = m_1 \ln(z - z_1) + m_1 \ln\left(\frac{a^2}{z} - \bar{z}_1\right)$$

or

$$w = -m_1 \ln z + m_1 \ln(z - z_1) + m_1 \ln\left(z - \frac{a^2}{\bar{z}_1}\right) + \text{const.}$$

equivalent to: a sink at the point z_1, a sink at the point $\frac{a^2}{\bar{z}_1}$, and a source at the origin.

APPENDIX 2

A four-dimensional Newton-Raphson algorithm has been used to solve the system of equations (32), (33), (34), and (35) for R_1, θ_1, K_0, K_1 after elimination of M_1 from equation (49).

```
      PROGRAM NR4D
      REAL K0,K1,K,J2,J3,J4,J5,J6,J7,I1,I2,I3,I4,I5,I6,I7,I8,I9
C-----------------------------------------------------------------------
C     DATA
C-----------------------------------------------------------------------
      ALFA=?
      ALF=ALFA*3.14159/180.0
   30 WRITE (5,110)
  110 FORMAT ( ' GIVE UNDERRELAXATION FACTOR')
      READ (5,120) C
  120 FORMAT (E)
C     T=THETA,  R=R1
      R=?
      T=?
      K0=?
      K1=?
   10 WRITE (5,100) R,T,K0,K1
  100 FORMAT  (4E15.6)
C-----------------------------------------------------------------------
      T1=6*T+2*ALF
      T2=2*T-2*ALF
      T3=T+ALF
      K=K0+K1
C-----------------------------------------------------------------------
      A1=2*R**4*(R*R-1)*(9*R*R-5)*COS(T)*COS(T1)
      A2=-4*R*R*(R*R-1)*(7*R*R-3)*COS(T)*COS(4*T)
      A3=2*(R*R-1)*(5*R*R-1)*COS(T)*COS(T2)
      A4=-2*R**4*(9*R**4-5)*SIN(T)*SIN(T1)
      A5=4*R*R*(7*R**4-3)*SIN(T)*SIN(4*T)-2*(5*R**4-1)*SIN(T)*SIN(T2)
      A6=-4*K0*R**5*(4*R*R-3)*SIN(T1)+8*K0*R**3*(3*R*R-2)*SIN(4*T)
      A7=-4*K0*R*(2*R*R-1)*SIN(T2)+12*K1*R**5*SIN(T1)
      A8=2*K1*R**3*(21*R*R-22)*SIN(4*T)+14*K1*R**3*(3*R*R-2)*COS(4*T)
      A9=8*K1*R*(3*R*R-1)*SIN(T2)+12*K1*R*(2*R*R-1)*COS(T2)
      B1=6*R*(K1+K*TAN(ALF))*(COS(4*ALF)-SIN(4*ALF))
      B2=-12*R**5*K*TAN(ALF)*COS(T1)
      B3=3*K*R**3*(14*R*R-4)*TAN(ALF)*COS(4*T)
      B4=14*K*R**3*(3*R*R-2)*TAN(ALF)*SIN(T)
      B5=K*R*TAN(ALF)*(8*(3*R*R-2)*COS(T2)+12*(2*R*R-1)*SIN(T2))
C-----------------------------------------------------------------------
      A11 = A1+A2+A3+A4+A5+A6+A7+A8+A9+B1+B2+B3+B4+B5
C-----------------------------------------------------------------------
      B6=-2*R**5*(R*R-1)**2*(SIN(T)*COS(T1)+6*COS(T)*SIN(T1))
      B7=4*R**3*(R*R-1)**2*(SIN(T)*COS(4*T)+4*COS(T)*SIN(4*T))
      B8=-2*R*(R*R-1)**2*(SIN(T)*COS(T2)+2*COS(T)*SIN(T2))
      B9=-2*R**5*(R**4-1)*(COS(T)*SIN(T1)+6*SIN(T)*COS(T1))
      C1=4*R**3*(R**4-1)*(COS(T)*SIN(4*T)+4*SIN(T)*COS(4*T))
      C2=-2*R*(R**4-1)*(COS(T)*SIN(T2)+2*SIN(T)*COS(T2))
      C3=-12*K0*R**6*(R*R-1)*COS(T1)+16*K0*R**4*(R*R-1)*COS(4*T)
      C4=-4*K0*R*R*(R*R-1)*COS(T2)+12*K1*R**6*COS(T1)
      C5=4*K1*R**4*(7*R*R-11)*COS(4*T)-28*K1*R**4*(R*R-1)*SIN(4*T)
      C6=4*K1*R*R*(3*R*R-2)*COS(T2)-12*K1*R*R*(R*R-1)*SIN(T2)
      C7=4*K*R**4*TAN(ALF)*(3*R*R*SIN(T2)-(7*R*R-3)*SIN(4*T))
      C8=28*K*R**4*(R**2-1)*TAN(ALF)*COS(4*T)
      C9=-4*K*R*R*TAN(ALF)*((3*R*R-4)*SIN(T2)-3*(R*R-1)*COS(T2))
C-----------------------------------------------------------------------
      A12 = B6+B7+B8+B9+C1+C2+C3+C4+C5+C6+C7+C8+C9
C-----------------------------------------------------------------------
      D1=-2*R**6*(R*R-1)*SIN(T1)+4*R**4*(R*R-1)*SIN(4*T)
      D2=-2*R*R*(R*R-1)*SIN(T2)
```

```
      D3=3*(R*R-1)*TAN(ALF)*(COS(4*ALF)-SIN(4*ALF))
      D4=-2*R**6*TAN(ALF)*COS(T1)+R**4*(7*R*R-3)*TAN(ALF)*COS(4*T)
      D5=7*R**4*(R*R-1)*TAN(ALF)*SIN(T)
      D6=2*R*R*(3*R*R-4)*TAN(ALF)*COS(T2)
      D7=6*R*R*(R*R-1)*TAN(ALF)*SIN(T2)
C-----------------------------------------------------------------
      A13=D1+D2+D3+D4+D5+D6+D7
C-----------------------------------------------------------------
      D8=2*R**6*SIN(T1)+R**4*(7*R*R-11)*SIN(4*T)
      D9=7*R**4*(R*R-1)*COS(4*T)+2*R*R*(3*R*R-2)*SIN(T2)
      E1=6*R*R*(R*R-1)*COS(T2)
      E2=3*(1+TAN(ALF))*(R*R-1)*(COS(4*ALF)-SIN(4*ALF))
      E3=-2*R**6*TAN(ALF)*COS(T1)+R**4*(7*R*R-3)*TAN(ALF)*COS(4*T)
      E4=7*R**4*(R*R-1)*TAN(ALF)*SIN(T)
      E5=2*R*R*TAN(ALF)*((3*R*R-4)*COS(T2)+3*(R*R-1)*SIN(T2))
C-----------------------------------------------------------------
      A14=D8+D9+E1+E2+E3+E4+E5
C-----------------------------------------------------------------
      E6=2*R**4*(R*R-1)*(9*R*R-5)*COS(T)*SIN(T1)
      E7=-4*R*R*(R*R-1)*(7*R*R-3)*COS(T)*SIN(4*T)
      E8=2*(R*R-1)*(5*R*R-1)*COS(T)*SIN(T2)
      E9=2*R**4*(9*R**4-5)*SIN(T)*COS(T1)
      G1=-4*R*R*(7*R**4-3)*SIN(T)*COS(4*T)+2*(5*R**4-1)*SIN(T)*COS(T2)
      G2=4*K0*R**5*(4*R*R-3)*COS(T1)-8*K0*R**3*(3*R*R-2)*COS(4*T)
      G3=4*K0*R*(2*R*R-1)*COS(T2)-12*K1*R**5*COS(T1)
      G4=-2*K1*R**3*((21*R*R-22)*COS(4*T)+7*(3*R*R-2)*SIN(4*T))
      G5=-4*K1*R*(2*(3*R*R-1)*COS(T2)+3*(2*R*R-1)*SIN(T2))
      G6=-6*(K1-K*TAN(ALF))*R*(COS(4*ALF)-SIN(4*ALF))
      G7=-12*K*R**5*TAN(ALF)*SIN(T1)
      G8=K*R**3*TAN(ALF)*(3*(14*R*R-4)*SIN(4*T)+14*(3*R*R-2)*COS(4*T))
      G9=4*K*R*TAN(ALF)*(2*(3*R*R-2)*SIN(T2)+3*(2*R*R-1)*COS(T2))
C-----------------------------------------------------------------
      A21 = E6+E7+E8+E9+G1+G2+G3+G4+G5+G6+G7+G8+G9
C-----------------------------------------------------------------
      I1=2*R**5*(R*R-1)**2*(-SIN(T)*SIN(T1)+6*COS(T)*COS(T1))
      I2=-4*R**3*(R*R-1)**2*(-SIN(T)*SIN(4*T)+4*COS(T)*COS(4*T))
      I3=2*R*(R*R-1)**2*(-SIN(T)*SIN(T2)+2*COS(T)*COS(T2))
      I4=2*R**5*(R**4-1)*(COS(T)*COS(T1)-6*SIN(T)*SIN(T1))
      I5=-4*R**3*(R**4-1)*(COS(T)*COS(4*T)-4*SIN(T)*SIN(4*T))
      I6=2*R*(R**4-1)*(COS(T)*COS(T2)-2*SIN(T)*SIN(T2))
      I7=-4*K0*R*R*(R*R-1)*(3*R**4*SIN(T1)+SIN(T2)-4*R*R*SIN(4*T))
      I8=4*K1*R**4*(3*R*R*SIN(T1)+(7*R*R-11)*SIN(4*T))
      I9=-4*K1*R*R*(7*R*R*(R*R-1)*COS(4*T)-(3*R*R-2)*SIN(T2))
      P1=-12*K1*R*R*(R*R-1)*COS(T2)
      P2=-4*K*R**4*TAN(ALF)*(3*R*R*COS(T1)-(7*R*R-3)*COS(4*T))
      P3=-28*K*R**4*(R**2-1)*TAN(ALF)*SIN(4*T)
      P4=4*K*R*R*TAN(ALF)*((3*R*R-4)*COS(T2)-3*(R*R-1)*SIN(T2))
C-----------------------------------------------------------------
      A22 = I1+I2+I3+I4+I5+I6+I7+I8+I9+P1+P2+P3+P4
C-----------------------------------------------------------------
      P5=2*R*R*(R*R-1)*(R**4*COS(T1)-2*R*R*COS(4*T)+COS(T2))
      P6=3*(R*R-1)*TAN(ALF)*(COS(4*ALF)-SIN(4*ALF))
      P7=-2*R**6*TAN(ALF)*SIN(T1)
      P8=R**4*TAN(ALF)*((7*R*R-3)*SIN(4*T)+7*(R*R-1)*COS(4*T))
      P9=2*R*R*TAN(ALF)*((3*R*R-4)*SIN(T2)+3*(R*R-1)*COS(T2))
C-----------------------------------------------------------------
      A23=P5+P6+P7+P8+P9
C-----------------------------------------------------------------
      Q1=-R**4*(2*R*R*COS(T1)+(7*R*R-11)*COS(4*T)+7*(R*R-1)*SIN(4*T))
      Q2=-2*R*R*((3*R*R-2)*COS(T2)+3*(R*R-1)*SIN(T2))
```

```
        Q3=-3*(1-TAN(ALF))*(R*R-1)*(COS(4*ALF)-SIN(4*ALF))
        Q4=-2*R**6*TAN(ALF)*SIN(T1)
        Q5=R**4*TAN(ALF)*((7*R*R-3)*SIN(4*T)+7*(R*R-1)*COS(4*T))
        Q6=2*R*R*TAN(ALF)*((3*R*R-4)*SIN(T2)+3*(R*R-1)*COS(T2))
C-----------------------------------------------------------------
        A24=Q1+Q2+Q3+Q4+Q5+Q6
C-----------------------------------------------------------------
        A31=2*(2*SIN(ALF)-K)*(R-COS(T3))+2*K1*R+2*K*TAN(ALF)*SIN(T3)
        A32=2*R*(2*SIN(ALF)-K)*SIN(T3)+2*K*R*TAN(ALF)*COS(T3)
        A33=-(1+R*R-2*R*COS(T3))+2*R*TAN(ALF)*SIN(T3)
        A34=-(1+R*R-2*R*COS(T3))+R*R-1+2*R*TAN(ALF)*SIN(T3)
C-----------------------------------------------------------------
        A41=2*(2*SIN(ALF)+K)*(R+COS(T3))+2*K*TAN(ALF)*SIN(T3)-2*K1*R
        A42=2*K*R*TAN(ALF)*COS(T3)-2*R*(2*SIN(ALF)+K)*SIN(T3)
        A43=1+R**2+2*R*COS(T3)+2*R*TAN(ALF)*SIN(T3)
        A44=1+R**2+2*R*COS(T3)+2*R*TAN(ALF)*SIN(T3)-(R*R-1)
C-----------------------------------------------------------------
        FA=2*R*(R*R-1)**2*COS(T)*(R**4*COS(T1)-2*R*R*COS(4*T)+COS(T2))
        FB=-2*R*(R**4-1)*SIN(T)*(R**4*SIN(T1)-2*R*R*SIN(4*T)+SIN(T2))
        FC=-2*K0*R*R*(R*R-1)*(R**4*SIN(T1)-2*R*R*SIN(4*T)+SIN(T2))
        FD=2*K1*R**6*SIN(T1)
        FE=K1*R**4*((7*R*R-11)*SIN(4*T)+7*(R*R-1)*COS(4*T))
        FG=2*K1*R*R*((3*R*R-2)*SIN(T2)+3*(R*R-1)*COS(T2))
        FH=3*(K1+K*TAN(ALF))*(R*R-1)*(COS(4*ALF)-SIN(4*ALF))
        FI=-2*K*R**6*TAN(ALF)*COS(T1)
        FJ=K*R**4*TAN(ALF)*((7*R*R-3)*COS(4*T)+7*(R*R-1)*SIN(4*T))
        FK=2*K*R*R*TAN(ALF)*((3*R*R-4)*COS(T2)+3*(R*R-1)*SIN(T2))
C-----------------------------------------------------------------
        F1 = FA+FB+FC+FD+FE+FG+FH+FI+FJ+FK
C-----------------------------------------------------------------
        FL=2*R*(R*R-1)**2*COS(T)*(R**4*SIN(T1)-2*R*R*SIN(4*T)+SIN(T2))
        FM=2*R*(R**4-1)*SIN(T)*(R**4*COS(T1)-2*R*R*COS(4*T)+COS(T2))
        FN=2*K0*R*R*(R*R-1)*(R**4*COS(T1)-2*R*R*COS(4*T)+COS(T2))
        FO=-2*K1*R**6*COS(T1)
        FP=-K1*R**4*((7*R*R-11)*COS(4*T)+7*(R*R-1)*SIN(4*T))
        FQ=-2*K1*R*R*((3*R*R-2)*COS(T2)+3*(R*R-1)*SIN(T2))
        FR=-3*(K1-K*TAN(ALF))*(R*R-1)*(COS(4*ALF)-SIN(4*ALF))
        FS=-2*K*R**6*TAN(ALF)*SIN(T1)
        FT=K*R**4*TAN(ALF)*((7*R*R-3)*SIN(4*T)+7*(R*R-1)*COS(4*T))
        FU=2*K*R*R*TAN(ALF)*((3*R*R-4)*SIN(T2)+3*(R*R-1)*COS(T2))
C-----------------------------------------------------------------
        F2 = FL+FM+FN+FO+FP+FQ+FR+FS+FT+FU
C-----------------------------------------------------------------
        FV=(2*SIN(ALF)-K)*(1+R*R-2*R*COS(T3))
        FW=K1*(R**2-1)+2*K*R*TAN(ALF)*SIN(T3)
        F3=FV+FW
        FX=(2*SIN(ALF)+K)*(1+R*R+2*R*COS(T3))
        FY=2*K*R*TAN(ALF)*SIN(T3)-K1*(R*R-1)
        F4=FX+FY
C***************************************************************************
        S1=A11*A22*(A33*A44-A43*A34)+A11*A23*(A32*A44-A42*A34)
        S2=A11*A24*(A32*A43-A42*A33)+A12*A21*(A33*A44-A43*A34)
        S3=A12*A23*(A31*A44-A34*A41)+A12*A24*(A31*A43-A41*A33)
        S4=A13*A21*(A32*A44-A34*A42)+A13*A22*(A31*A44-A34*A41)
        S5=A13*A24*(A31*A42-A41*A32)+A14*A21*(A32*A43-A33*A42)
        S6=A14*A22*(A31*A43-A33*A41)+A14*A23*(A31*A42-A41*A32)
        DET = S1+S2+S3+S4+S5+S6
C-----------------------------------------------------------------
        J2=F1*A22*(A33*A44-A43*A34)+F1*A23*(A32*A44-A42*A34)
        J3=F1*A24*(A32*A43-A42*A33)+A12*F2*(A33*A44-A43*A34)
```

76

```
          J4=A12*A23*(F3*A44-A34*F4)+A12*A24*(F3*A43-F4*A33)
          J5=A13*F2*(A32*A44-A34*A42)+A13*A22*(F3*A44-A34*F4)
          J6=A13*A24*(F3*A42-F4*A32)+A14*F2*(A32*A43-A33*A42)
          J7=A14*A22*(F3*A43-A33*F4)+A14*A23*(F3*A42-F4*A32)
          H1 = (J2+J3+J4+J5+J6+J7) / DET
C-------------------------------------------------------------------
          U1=A11*F2*(A33*A44-A43*A34)+A11*A23*(F3*A44-F4*A34)
          U2=A11*A24*(F3*A43-F4*A33)+F1*A21*(A33*A44-A43*A34)
          U3=F1*A23*(A31*A44-A34*A41)+F1*A24*(A31*A43-A41*A33)
          U4=A13*A21*(F3*A44-A34*F4)+A13*F2*(A31*A44-A34*A41)
          U5=A13*A24*(F4*A31-F3*A41)+A14*A21*(F3*A43-F4*A42)
          U6=A14*F2*(A31*A43-A33*A41)+A14*A23*(F4*A31-F3*A41)
          H2 = (U1+U2+U3+U4+U5+U6) / DET
C-------------------------------------------------------------------
          V1=A11*A22*(F3*A44-F4*A34)+A11*F2*(A32*A44-A42*A34)
          V2=A11*A24*(A32*F4-A42*F3)+A12*A21*(F3*A44-F4*A34)
          V3=A12*F2*(A31*A44-A34*A41)+A12*A24*(A31*F4-A41*F3)
          V4=F1*A21*(A32*A44-A34*A42)+F1*A22*(A31*A44-A34*A41)
          V5=F1*A24*(A31*A42-A41*A32)+A14*A21*(A32*F4-F3*A42)
          V6=A14*A22*(A31*F4-F3*A41)+A14*F2*(A31*A42-A41*A32)
          H3= (V1+V2+V3+V4+V5+V6)/ DET
C-------------------------------------------------------------------
          W1=A11*A22*(A33*F4-A43*F3)+A11*A23*(A32*F4-A42*F3)
          W2=A1*F2*(A32*A43-A42*A33)+A12*A21*(A33*F4-A43*F3)
          W3=A12*A23*(A31*F4-A41*F3)+A12*F2*(A31*A43-A41*A33)
          W4=A13*A21*(A32*F4-A42*F3)+A13*A22*(A31*F4-A41*F3)
          W5=A13*F2*(A31*A42-A41*A32)+F1*A21*(A32*A43-A33*A42)
          W6=F1*A22*(A31*A43-A33*A41)+F1*A23*(A31*A42-A41*A32)
          H4 = (W1+W2+W3+W4+W5+W6)/ DET
C-------------------------------------------------------------------
          R =R-C*H1
          T =T-C*H2
          K0=K0-C*H3
          K1=K1-C*H4
          IF(ABS(H1).LT.1.E-3.AND.ABS(H2).LT.1.E-3)GO TO 20
          IF(ABS(H3).LT.1.E-3.AND.ABS(H4).LT.1.E-3) GO TO 20
          GO TO 10
   20     WRITE (5,100) R,T,K0,K1
          WRITE (5,130)
  130     FORMAT ( ' IF YOU WANT ANOTHER RELAXATION FACTOR, TYPE 1')
          READ (5,140) IFF
  140     FORMAT (I)
          IF (IFF.EQ.1) GO TO 30
          STOP
          END
```

1. Report No.	2. Government Accession No.	3. Recipient's Catalog No.
NASA CR-177347		

4. Title and Subtitle	5. Report Date
ANALYSIS OF SELECTED PROBLEMS INVOLVING VORTICAL FLOWS	April 1985
	6. Performing Organization Code

7. Author(s)	8. Performing Organization Report No.
L. Roberts, D. L. Lee and N. Mourtos	
	10. Work Unit No.

9. Performing Organization Name and Address	11. Contract or Grant No.
Dept. of Aeronautics/Astronautics Stanford University Stanford, CA 94305	NCC 2-149
	13. Type of Report and Period Covered

12. Sponsoring Agency Name and Address	Contractor Report
National Aeronautics and Space Administration Washington, D. C. 20546	14. Sponsoring Agency Code
	RTOP #505-42-11

15. Supplementary Notes

Point of Contact: Technical Monitor:Dr. Sanford Davis, M/S 227-8
Ames Research Center, Moffett Field,
CA 94035

16. Abstract

Analyses are presented for three selected problems involving vortical flows; namely (i) the persistence and decay of trailing vortex, (ii) the interaction between a rotor tip vortex and a following blade including the acoustic field generated, and (iii) the flow over a flat plate with a detached vortex/sink. Emphasis is placed on obtaining analytical solutions including those cases where the effects of turbulence is important to a proper description of the flow.

17. Key Words (Suggested by Author(s))	18. Distribution Statement
Vortex flows Blade vortex interaction Detached vortices	Unclassified – Unlimited STAR Category 02

19. Security Classif. (of this report)	20. Security Classif. (of this page)	21. No. of Pages	22. Price*
Unclassified	Unclassified	77	A05

*For sale by the National Technical Information Service, Springfield, Virginia 22161

END

DATE

FILMED

JUL 22 1985

End of Document